2011

Crack formation in investment casting ceramic shells

W. A. Everhart

Department:

CRACK FORMATION IN INVESTMENT CASTING CERAMIC SHELLS

by

WESLEY ALEXANDER EVERHART

A Thesis

Presented to the Faculty of the Graduate School of the

MISSOURI UNIVERSITY OF SCIENCE AND TECHNOLOGY

In Partial Fulfillment of the Requirements for the Degree

MASTER OF SCIENCE IN METALLURGICAL ENGINEERING

2011

Approved by

Von L. Richards

Simon Lekakh

K. Chandrashekhara

PUBLICATION THESIS OPTION

This thesis consists of the following three papers that have been prepared in accordance with their perspective publishers stipulations and have been submitted and/or accepted for publication as follows:

Paper I (Pages 12-32) has been submitted to the Journal of Materials Processing Technology.

Paper II (Pages 33-53) has been submitted to the AFS Transactions.

Paper III (Pages 54-71) has been submitted to the Journal of Engineering Fracture Mechanics.

ABSTRACT

This thesis is a collection of papers that discuss shell cracking in investment casting during pattern removal. The application of rigid polymeric foam for large investment casting patterns with complex geometries can improve the dimensional tolerances and the surface quality of the casting. However, these pattern materials have a tendency to promote crack formation in investment casting shells during pattern removal by firing.

The first two papers discuss the factors affecting shell cracking and methods to prevent it. Experimental methods were combined with finite element modeling to predict stress in the shell. A 3D nonlinear finite element model was developed to predict possible crack formation in the shells during pattern removal. The effects of the thermo-mechanical properties of the foam and the shell, as well as the firing process parameters were modeled. Also, an experimentally measured delay of the thermal expansion of the pattern was incorporated in the model to simulate the effect of aging. Extreme cases were experimentally validated. Recommendations for firing process parameters and pattern design to decrease stress and eliminate crack formation in the shell were formulated.

The third paper discusses the strength of investment casting shells in corner regions. The corner and edge regions have different structure and thickness and can experience large mechanical stress during processing. Experimental methods were combined with finite element modeling to predict stress in edge regions of the shell. A general equation was developed to account for these variables. The model was experimentally verified with wedge tests for various cases.

ACKNOWLEDGEMENTS

I would like to thank Dr. Von Richards and Dr. Simon Lekakh for their continuous help and support throughout this research. Their guidance had been a great motivational force for me.

I wish to express my gratitude to Dr. K. Chandrashekhara, Dr. Jian Chen, and graduate student Haifeng Li for their work on the modeling for this thesis.

I would like to thank US Army ARDEC - Benet Labs for providing funding for this research. I also acknowledge the support of Steel Founders Society of America.

I would like to thank Dr. Smith for his assistance and graduate students Chirag Mahimkar, and Darryl Kline for their assistance with equipment. I also thank Jamie Fitzgerald, Tom Towey, and Katherine Ramsey for their assistance in sample preparation.

Finally, I would like to thank my parents, sister and friends for their support.

TABLE OF CONTENTS

Page

LIST OF ILLUSTRATIONS

LIST OF TABLES

1. INTRODUCTION

1.1. BACKGROUND

The investment casting process is generally used to produce small, thin walled castings with high detail. The process starts with the manufacture of a pattern. The most common material for patterns is wax but different types of polymeric patterns are also used[1-2]. The pattern is dipped in slurry made of ceramic binder and flour usually containing some combination of fused silica, zircon, alumina, or other ceramic material. Refractory granules referred to as stucco are then applied to the wet slurry coating. The combination of slurry and stucco makes a single coat which is allowed to dry before the next coat is applied. The shell building process generally consists of one or two prime coats, designed to provide a better surface finish for the casting, four to ten back up coats, designed to add strength to the shell, and a seal coat, designed to seal the stucco of the final backup coat[3-7]. The pattern is then removed from the shell by melting or decomposition in an autoclave or furnace. Whether done as a part of pattern removal, or as an additional firing process, the ceramic is sintered to increase the strength of the shell enough to hold the pressure of liquid metal. Liquid metal is then poured into the shell, which is usually preheated.

Large patterns made from wax often do not have the strength necessary to hold their shape due to their higher weight, especially in situations where the pattern has unsupported extensions, which can lead to creep[8]. These are reasons for the use of polymeric foam as a pattern material in investment casting. Some of the first foams used were expanded polystyrene (EPS) foams[9]. This material has much lower density than wax and, despite its lower strength, can support its own weight much better in larger

patterns. This becomes especially important to the dimensional stability of the pattern when stored. EPS foams are also very buoyant which causes problems when the pattern is initially dipped in the slurry. The forces on the pattern when submerged can be high enough to distort or break the pattern. Because of this issue, stronger, higher density polymeric foams are needed. Polyurethane foams fit these requirements well and can be made in complicated shapes with high surface quality and dimensional accuracy[10]. However, polyurethane foams have high thermal expansion and a high decomposition temperature which can cause the pattern to expand and break the shell during the pattern removal process[9]. Due to the majority of these cracks forming along the edges and in the corners of the shell the properties of these areas are also of interest.

1.2. REVIEW OF LITERATURE

1.2.1. Factors Affecting Shell Cracking. There has been a large amount of work done to investigate the factors that cause shell cracking. Most of this work has been involved with the removal of wax patterns from the mold.

It has been shown that the thermal expansion of the pattern has a large impact on the chances of cracking when using wax patterns. With a simple comparison of the thermal expansion of the wax and shell within the working temperature range of the wax, shells will have a high probability of cracking during pattern removal[11, 12]. It can be concluded from this observation that using a pattern material with low melting temperature and a low coefficient of thermal expansion can reduce the chance of shell cracking by reducing the total amount of thermal expansion in the wax[11, 13, 14]. The low thermal conductivity and diffusivity of the wax allows for the external portion of the wax to melt first. This provides the opportunity for the liquid wax on the surface of the

pattern to flow into the shell relieving any stresses that had been developed[11, 15]. It has also been shown that the viscosity of the wax has a significant effect on the chances of shell cracking[16]. The viscosity of the wax affects its ability to transfer load, similar to the elastic modulus of a solid. Higher viscosities can increase the chances of shell cracking[2].

Some work has been done with stereolithography patterns and other rapid prototyping materials[2, 17]. Yao and Leu[17] studied shell cracking in investment casting shells during burnout of laser stereolithography patterns. The factors considered in this study include the buckling temperature of the pattern, and the glass transition temperature of the epoxy resin. The work shows that if the shell survives until the temperature is above the glass transition temperature and the buckling temperature than the shell will not crack.

Much of the previous work discusses the effect of melting rate on the chances of shell cracking when using wax patterns. Buntrock[17] shows that the key to successful dewaxing in an autoclave relies on high pressure as well as elevated temperature to melt the outside surface of the wax before enough pressure has built up to break the shell. Flash firing relies on only high temperature to accomplish the same goal. Both methods can be used to successfully remove wax patterns from investment casting molds. Foster[1] discusses the method and advantages of using flash firing to remove any pattern material. The range of temperatures recommended for flash firing was 760 – 1800 °C. Some advantages of flash firing include high repeatability, the combination of de-waxing and burnout into one process for wax patterns, and less shell cracking. Ceriotti[13] discusses the best ways to avoid shell cracking during mold firing and prefiring. To limit the effect of a materials with a high coefficient of thermal expansion, higher heating rates, like

those achieved from flash firing, should be used[13, 9]. While the mold and pattern heat up in the furnace there is a thermal gradient from the outside of the shell to the inside of the pattern which reduces the amount material that is expanded.

While little work has been done on shell cracking from pattern removal of polyurethane foam patterns, several conclusions can be drawn from the works above. To remove the pattern from the mold without shell cracking, the pattern and shell should be rapidly heated to create a thermal gradient within the materials. This minimizes the amount of thermal expansion of the pattern regardless of mold or shell properties. Additionally, the minimization of the pattern melting (or decomposition) temperature, coefficient of thermal expansion and elastic modulus reduce the chance of shell cracking. Materials with low coefficients of thermal expansion will tend to have higher decomposition temperatures requiring compromise between these two properties.

1.2.2. Polyurethane Foam Properties. The properties of the pattern are important to consider when investigating shell cracking. This work investigates the use of polyurethane foam patterns. The properties that most affect the chances of shell cracking are decomposition temperature, coefficient of thermal expansion, density, elastic modulus, and glass transition temperatures.

Yan et al.[18] studied the thermal degradation of rigid polyurethane foams. Their study used thermal gravimetric analysis to show that the decomposition of the foam takes place between 250 and 400 °C.

Zhang et al.[19] studied the thermal expansion of various polymeric foams. They found that 62 kg/m^3 polyurethane foam expands approximately 7% between 30 and 140 °C. It was also shown that the foam applied some pressure during expansion and that

compressing the foam prior to heating could increase both the amount of expansion and the pressure from the expanding foam. The coefficient of thermal expansion of various foams was studied and showed that rigid polyurethane foam has a coefficient of thermal expansion of approximately 120 x 10^{-6} (20-125°C) and that expanded polystyrene foam has a coefficient of thermal expansion of 75 x 10^{-6} (20-72 °C) [9].

Several studies have been done on the mechanical properties of polyurethane foam. There is large variation in the densities of foam that were used which is likely the cause of high variation in the reported elastic modulus (Table 1).

Table 1.1. Density and elastic modulus of various polyurethane foams.

Author	Density, kg/m^3	Elastic Modulus, MPa
Kline et al. [9]	150	7.4
Abbas et al. [20]	166	35
Calvert et al. [21]	24-641	115-800

Several studies have been done on the physical properties of polyurethane foam such as glass transition temperatures and their effect on other properties. Glass transition temperatures have been shown at 60 °C[22] and 150 °C[23]. It has been shown that crystallinity of the sample can hinder detection of these glass transition temperatures[22]. It has also been suggested that a relationship between glass transition temperatures and the aging of polyurethane foam exists[23]. Room temperature aging showed no significant effect, but aging at elevated temperature can show up to a 2% volume change[23].

1.2.3. Thermo-physical Properties. The thermo-physical properties of the investment casting shell and polyurethane foam pattern are important when trying to understand or model how shell cracking occurs.

Several studies have been done to determine the heat capacity and thermal conductivity of various investment casting shells. Changes in the materials, the slurry viscosity, or other shell building variables can have an effect on these properties. Shells that were built using colloidal silica binder, fused silica flour and fused silica stucco, similar to the shells used in this thesis, are summarized in Table 2.

Table 1.2. Thermal conductivity and heat capacity of various investment casting shells.

Author	Test Method	Thermal Conductivity, W/mK	Heat Capacity, J/gK
Kline et al. [9]	Hot Wire	0.55	1.0
Kruse and Richards [14]	Extrapolated from Shell Saturation	0.6-1.4	-
Sabau and Viswanathan [24]	Hot Wire and Laser Flash	0.65	0.54
Drushitz et al. [25]	Hot Wire	0.55	-
Mahimkar et al. [26]	Laser Flash	0.65	1.0

1.2.4. Shell Structure. Due to a majority of cracks in investment casting shells occurring in the corner and edge regions, work has been done to compare properties in these regions to properties in flat regions. Hyde et al.[27] studied the difference in properties of edge and flat regions in investment casting shells. The authors developed the following equation to determine the breaking stress of wedge shell samples:

$$\sigma = \frac{12.2Fd \sin\theta \cos\theta}{WT^2} \quad (1)$$

It was determined that the wedge requires less force to break due to stress concentration at the corner and that the wedge samples are more sensitive to flaws in the structure of the shell located in the area of failure. Jones et al.[28] used this test and the published[27] equation in their study. Results showed that the corners of the shells were weaker than the flat samples. Isobe et al.[29] studied the effect of various amounts and sizes of porosity on the mechanical properties investment casting shells. They showed that the stress concentration caused by pores is similar to the stress concentration seen in corners. They also showed that 3-point bend strength is proportional to pore size in the sample. Larger pores lower the strength of the sample more significantly.

Recently published experimental strength and porosity data of various porous ceramics were reviewed[30] and these data were compared with values calculated from both the minimum contact solid area (MCA) and the pore stress concentration effect (SCE) models[8]. According to the MCA model, the mechanical strength of fully dense ceramic decreases exponentially with increase in volume fraction porosity (P):

$$\sigma = \sigma_0 exp(-bP) \tag{2}$$

where: b is an empirical parameter related to the minimum solid area and dependent on the pore structure.

According to the SCE model, the resulting fracture strength-porosity relationship for all ceramic materials can be given by a power equation of the form:

$$\sigma = \sigma_0 (1 - P)^{\eta} \tag{3}$$

where: η is related directly to the pore structure (shape and orientation of the pores with respect to the stress axis) and the Poisson's ratio of the material.

It was observed that the MCA model matched the experimental results of ceramics in the low volume fraction porosity range ($P < 0.25$) range, whereas in the volume fraction porosity range ($P > 0.35$), the SCE model better predicts the experimental results[8]. Because investment casting shells have a volume fraction of porosity around 0.3, both models could be used to predict the flexural breaking stress in flat regions typically obtained from three or four-points bent tests[8]. It could be assumed that interference of both types of concentrators, corner radius of the investment shell and its internal pores, takes place and this interference will affect the overall stress development in the shell.

1.3. FOCUS OF RESEARCH

The objective of this research was to prevent crack formation in the green ceramic shell during polyurethane foam pattern removal. To achieve this goal, the thermo-mechanical properties of the polyurethane foam and ceramic shell were experimentally determined. These data were used in a finite element model that predicts crack formation during pattern removal. In addition, the effect of aging on the pattern was investigated and incorporated into the model. Due to the location of most cracks on the edges and corners of the shell of a test procedure was developed to determine the properties of investment casting shells in flat and edge regions and to investigate the effect of shell geometry (wall angle and corner radius) on the force required to break the shell. A combination of finite element modeling, experimental wedge testing and microstructural analysis was used to determine these effects. All modeling results were validated by experiments and recommendations were made on the investment casting process to minimize the chances of shell cracking during pattern removal.

REFERENCES

1. Foster, G, "Flashfire Dewax for Today's Investment Casting Foundry", Investment Casting Institute 42nd Annual Meeting, pp. 2:1-2:11, Atlanta, Georgia; USA; 25-28 September 1994.

2. Yao, W L; Leu, Ming C, "Analysis of Shell Cracking in Investment Casting with Laser Stereolithography Patterns", Rapid Prototyping Journal, Vol. 5, no. 1, March 1999.

3. Capadona, J A, "Slurry Process Control in Production can "Crack Down" on Shell Cracking", Incast Vol. 4, no. 4 pp. 10-12, April 1991.

4. Guerra, M, Schiefelbein, G W, "Review of Shell Components, Shell Characteristics and Properties: Refractory Selection for Primary Shell Coat", Investment Casting Institute 42nd Annual Meeting, Atlanta, Georgia; USA; 25-28 September 1994.

5. Arzt, A M, "Optimizing Control of Shell Cracking in Investment Casting", Mod. Cast. Vol. 77, no. 2, pp. 30-33. February 1987.

6. Roberts, W O, "Shell Cracking – a Complete and Detailed Compilation of Papers, Case Histories, and Discussions Presented at the AFS/CMI Symposium "Factors Affecting Shell Cracking", "Colloidal Silica", American Foundrymen's Society, Publications Department, Golf & Wolf Roads, Des Plaines, 1987.

7. Schiefelbein, G W, "Ceramic Shell Production for Controlling Shell Cracking", Conference on Factors Affecting Shell Cracking, December 2-3, 1986.

8. Cannell, N, Sabau, A S, "Predicting Pattern Tooling and Casting Dimensions for Investment Casting, Phase II", Final technical report, September 2005.

9. Kline, D, Lekakh, S, Mahimkar, C, Richards, V, "Crack Formation in Ceramic Shell During Foam Pattern Firing", Technical and Operating Conference, Chicago, Illinois; USA; December 2009.

10. "Foam Patterns for Investment casting", Modern Casting, Vol. 99, no. 7, pp. 46, July 2009.

11. Ostrowski, R C, "Wax Properties that Affect Ceramic Shell Cracking", Conference on Factors Affecting Shell Cracking, December 1986.

12. Richards, V L, Rasquinha, D, Sunderland, B, "Investment Casting Shell Cracking," Steel Founder's Society Technical and Operating Conference Proceedings, November 2001.

13. Ceriotti, L L, "Factors Affecting Shell Cracking – Mold Firing and Prefiring", Conference on Factors Affecting Shell Cracking, December 1986.

14. Kruse, B L, Richards, V L, "Thermal and Moisture Characterization During Autoclave Dewaxing in Investment Casting", Investment Casting Institute 53rd Technical Conference and Exposition, November 2005.

15. Kruse, B L, Richards, V L, "The Success of a Data Acquisition System Designed to Measure Thermal, Moisture and Pressure Profiles in Production Autoclaves", Investment Casting Institute 53rd Technical Conference and Exposition, November 2005.

16. Whitehouse, C, Dahlin, Barry, "Effects of Wax Viscosity and Shell Permeability on Shell Cracking", Incast, Vol. 22, no. 4, April 2009.

17. Buntrock, K A, "Dewaxing Methods and Their Influence on Shell Cracking", Conference on Factors Affecting Shell Cracking, December 1986.

18. Yan, Y, Xu, J, Pang, H, Zhang, R, Liao, B, "Thermal Decomposition and Kinetics of Rigid Polyurethane Foam Derived from Sugarcane Bagasse", Journal of Wuhan University of Technology, 2009.

19. Zouguang, Z, Jijun, H, Zhijie, Min, Li, S, Yizou, G, "Thermal Expansion Process for Manufacturing of Stitched Sandwich Structures", Journal of Rienforced Plastics and Composits, Vol. 29, no. 9, pp.1418-1427, May 2010.

20. Niknejad, A, Liaghat, GH, Moslemi, N H, Behravesh, AH, "Theoretical and Experimental Studies of the Instantaneous Folding Force of the Polyurethane Foam-filled Square Honeycombs", Materials and Design. Vol. 32, no. 1, pp. 69-75, January 2011.

21. Calvert, K L, Trumble, K P, Webster, T J, Kirkpatrick, L A, "Characterization of Commercial Rigid Polyurethane Foams used as Bone Analogs for Implant Testing", Journal of Materials Science: Materials in Medicine, Vol. 21, no. 5, pp. 1453-1561, May 2010.

22. Li, X ; Cao, H, Zhang, Y, "Structures and Physical Properties of Rigid Polyurethane Foams with Water as the Sole Blowing Agent", Science in China. Series B, Chemistry, Vol. 49, no. 4, pp. 363-370, 2006.

23. Ho, T, Wynne, K J, "A New Fluorinated Polyurethane: Polymerization, Characterization, and Mechanical Properties", Macromolecules, pp.3521-3527, 1992

24. A. S. Sabau, S. Viswanathan, "Thermo-physical Properties of Zircon and Fused Silica Based Shells for Investment Casting", Transactions of the American Foundry Society, Vol. 112, No. 04-081, pp 649 - 661, 2004.

25. Druschitz, E A, Lekakh, S, Richards, V, "Modeling of Heat Transfer Through Investment Casting Shells: Method of Determining Shell Thermal Conductivity", Technical and Operating Conference, 2006.

26. C. Mahimkar, V. L. Richards, S.N. Lekakh, "High Temperature Thermo-physical Properties of Ceramic Shell", Missouri University of Science & Technology, ICI, 2009

27. Hyde, R, Leyland, S, Withey, P, Jones, S, "Evaluation of the Mechanical Properties of Investment casting Shells", 22nd Investment Casting Conference, 1995.

28. Jones, S, Yuan, C, Blackburn, S, "Fundamental Study on Microstructure and Physical Properties of Fluidized Bed and Rainfall Sanding Ceramic Shells", Materials Science and Technology, Vol. 23, no. 6, 2007.

29. Isobe, T, Kameshima, Y, Nakajima, A, Okada, K, Hotta, Y, "Gas Permeability and Mechanical Properties of Porous Alumina Ceramics with Unidirectionally Aligned Pores", Journal of the European Ceramic Society, Vol. 27, no. 1, pp. 53-59, 2007

30. Nyongesa, F W, Aduda, B O, "Fracture Strength of Porous Ceramics: Stress Concentration vs Minimum Solid Area Models", African Journal of Science and Technology, Science and Engineering Series, Vol. 5, no. 2, pp 19-27, December 2004.

PAPER

I. CRACK FORMATION DURING FOAM PATTERN FIRING IN THE INVESTMENT CASTING PROCESS

W.A. Everhart, S.N. Lekakh and V.L. Richards
Department of Materials Science and Engineering

J. Chen and K. Chandrashekhara
Department of Mechanical and Aerospace Engineering

Missouri University of Science and Technology, Rolla, MO 65409

(Submitted for Publication to the Journal of Materials Processing Technology, July 2011)
(Edited for thesis)

ABSTRACT

The application of rigid polymeric foam for large investment casting patterns with complex geometries can improve the dimensional tolerances and the surface quality of the casting. However, these pattern materials promote crack formation in investment casting shells during pattern removal using standard firing procedures. ASTM standard tests and independently developed experimental methods were combined with finite element modeling to predict stress development in the shell. The model takes into consideration the thermal properties of the pattern and the shell materials to determine the heat transfer within the materials to establish a thermal gradient. This is combined with mechanical properties to determine the thermal expansion stresses developed in the shell during firing. A 3D nonlinear finite element model was developed to predict possible crack formation in the shells during pattern removal. The effects of the thermo-mechanical properties of the foam and the shell, as well as the firing process parameters were modeled, and extreme cases were experimentally validated. Recommendations for firing process parameters and pattern design to decrease stress and eliminate crack formation in the shell were formulated.

Keywords: ceramic shell, investment casting, crack, stress modeling, molding

1. INTRODUCTION

The investment casting process is generally used to produce small, thin walled castings with high detail. The process begins with the manufacture of a pattern from an easily shaped, inexpensive material. The most common material for patterns is wax but different types of polymeric foam are also used[1-2]. The pattern is dipped in slurry made of inorganic binder and oxide flour usually containing some combination of fused silica, zircon, alumina, or other ceramic material. Refractory granules referred to as stucco (usually fused silica, zircon or alumina) are then applied to the wet slurry coating. The combination of slurry and stucco makes a single coat which is allowed to dry before subsequent coats are applied. The shell building process generally consists of three different types of layers. Prime coats are designed to provide a better surface finish for the casting and are applied first, usually in one or two coats. Backup coats are designed to add strength to the shell and are applied after any prime coats; four to ten backup coats are applied. The seal coat is designed to seal the stucco of the final backup coat and is applied last[3-7]. The pattern is then removed from the unfired or green shell by melting or decomposition in an autoclave or furnace. Whether done as a part of pattern removal, or as an additional firing process, the ceramic is sintered to increase the strength of the shell such that the pressure of liquid metal will not cause cracks. Liquid metal is then poured into the shell, which is usually preheated, to produce the casting.

Large patterns made from wax often do not have sufficient strength to hold their shape due to their higher weight, especially in situations where the pattern has unsupported extensions, leading to creep[8]. Polymeric foams were considered as pattern materials in investment casting in an attempt to overcome some of the wax deficiencies.

Some of the first foams used were expanded polystyrene (EPS) [9]. This material has much lower density than wax and, despite its lower strength, doesn't suffer from the self loading creep that is common with wax patterns, especially in larger patterns. This becomes especially important to the dimensional stability of the pattern during storage. However, EPS foams are also very buoyant which causes problems when the pattern is initially dipped in the slurry. The forces on the pattern when submerged can be high enough to distort or even break the pattern. EPS foam and wax patterns also show some dimensional change when they are cooled after production. Because of these issues, stronger, higher density polymeric foams are needed. Polyurethane foams fit these requirements well and can be made in complicated shapes with high surface quality and dimensional accuracy[10]. However, polyurethane foams have high coefficients of thermal expansion and high decomposition temperatures which can cause the pattern to expand and break the shell during the pattern removal process[9].

The objective of this research was to prevent crack formation in the green ceramic shell during polyurethane foam pattern removal. To achieve this goal, the thermo-mechanical properties of the polyurethane foam and ceramic shell were experimentally determined. These data were used in a finite element model that predicts crack formation during pattern removal. The modeling results were validated by experiments and recommendations were made on the investment casting process to minimize the chances of shell cracking during pattern removal.

2. PROCEDURES

Experimental. Polyurethane foam with density of 170 kg/m3 was tested. The properties of the polyurethane foam were compared to EPS foam with 26 kg/m3 density. Samples were cut from the center of foam blocks with a cross-section of 7000 mm2. Compression testing of the foam was done to determine the elastic modulus with varying pattern dimensions. Samples had a cross-section of 2580 mm2 and a thickness of 25.4 mm or 50.8 mm. Tests were run according to ASTM D1621[11]. Thermal gravimetric analysis (TGA) was carried out using a 2950 Thermo-gravimetric analyzer. Samples were tested in air from 30°C to 600°C using a constant heating rate of 10°C/min. The air flow rate was set to 100 ml/min. The thermal expansion of the foam was measured using a laser assisted dilatometer. Foam samples were cut into 50 mm long 18 mm diameter cylinders. Two thin aluminum disks were placed on both ends of the foam and inserted into a quartz glass tube (19 mm diameter) and then submerged in an oil bath. A small hole was present in the end of the tube to allow oil flow inside for improved heating of the sample. Another quartz tube was placed on the upper aluminum disk. The expansion of the foam sample was monitored through the linear movement of the upper tube using a laser proximity probe with 1 μm precision. The average temperature of the foam samples was collected by averaging the reading of two thermocouples inserted in the oil bath, one of which was inserted in a spare foam sample and the other thermocouple was left exposed to the oil. The heating rate of the foam was approximately 1°C/min.

A simple pattern (50.8 x 63.5 x 63.5 mm) was prepared to test shell cracking during burnout (Figure 1). The slurry was consisted of colloidal silica binder (Megasol BI) and fused silica flour (-200 mesh). The slurry viscosity was measured by a Brookfield

DVII+ Pro Viscometer. All coatings were applied at 800 ± 100 cP viscosity which is equivalent to 19-22 seconds on a #5 Zahn cup. The patterns were submerged in the slurry until completely covered and then removed and suspended over the slurry for approximately 50 seconds. During this time, the pattern was rotated and allowed to drain from different points to promote an even coating. A uniform distribution of stucco was then applied using the rainfall method. This was done by continuously rotating the pattern so that all surfaces were directly impacted by the falling stucco until no more stucco would adhere to the surface. The stucco for the prime coat was granular zircon (-100+200 mesh) and the stucco for the back-up coats was fused silica (-30+50 mesh). The seal coat used no stucco. The samples were dried for at least four hours between coats.

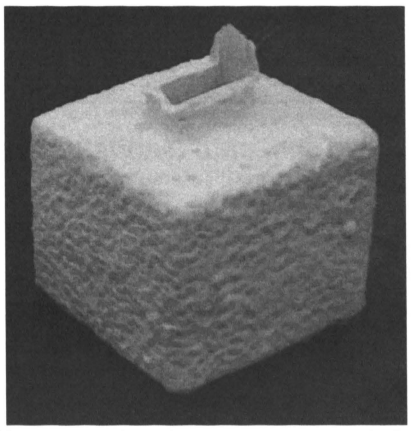

Figure 1. Shell built around a foam pattern: 50.8 x 63.5 x 63.5 mm.

Shells were fabricated with one prime coat, either three or five backup and one seal coat. The samples with three backup coats had five total layers (3.8 mm average thickness) and the samples with five backup coats had seven total layers (6.4 mm average thickness). After the seal coat was applied the samples dried for another 24 hours. All

experimental specimens were tested during the week after shell fabrication. Shells were fired in an electric box furnace using two different procedures: continuous heating from room temperature to 600°C at 3°C/min and flash firing in a furnace preheated to 600°C. The maximum stress at rupture and elastic modulus of the shells were determined using three point bend testing of "green" shells performed at room temperature according to ASTM C1161[12]. The tip of the testing fixture had a radius of 3 mm. Five samples of shells with five and seven layers were tested. The density of the shells was measured using Archimedes method in distilled water according ASTM C20 using approximately 10 g samples[13].

Modeling. A nonlinear coupled finite element model was developed to study crack formation in the shell during pattern removal. The model accounts for both mechanical and thermal loadings and assumes a fixed interface between the pattern and shell. It is capable of simulating the complete detail of pattern and shell behavior during the firing process. To reduce computational time, one quarter of the pattern surrounded by shell has been modeled and symmetric boundary conditions are applied at the cut planes. An eight-node brick element is used to mesh the model. To mesh the pattern, all edges are initially seeded by numbers. In order to obtain higher result accuracy and save computational cost, additional seeds and biased seeds are used in critical regions and fewer seeds in regions that are less of interest, and hex mesh shape and structured mesh technique are used. The mesh of the finite element model for both the shell and foam pattern is shown in Figure 2. Finer mesh is used near the corner of ceramic shell. 19,683 brick elements were used for the model. The contact properties between the pattern and shell are defined as fixed in order to simulate the actual experimental process.

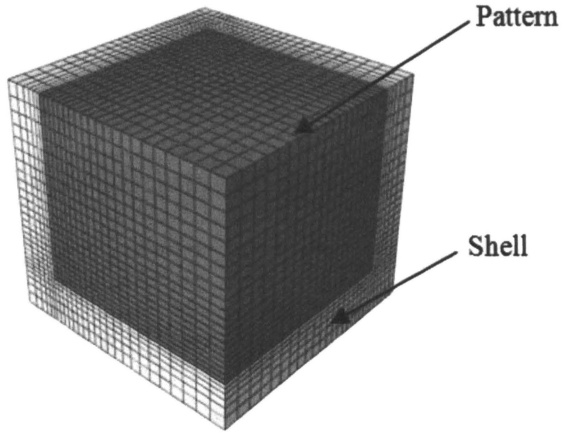

Figure 2. Mesh of finite element model for the foam pattern and ceramic shell.

The formulation for the transient mechanical analysis can be written as:

$$[M^e]\{\ddot{U}^e\} + [K^e]\{U^e\} = \{F^e\} + \{F_T^e\} \quad (1)$$

where: $[M^e] = \int_V \rho[N]^T[N]dV$

$[K^e] = \int_V [B]^T[C][B]dV$

$\{U^e\} = \{u, v, w\}^T$

$[M^e]$ is the mass matrix, $[K^e]$ is the stiffness matrix, $\{F^e\}$ and $\{F_T^e\}$ are mechanical and thermal loadings, N is the shape function, B is the strain-displacement function, C is the elasticity matrix, ρ is the density, and $\{u, v, w\}^T$ are displacement components in a rectangular Cartesian coordinate system.

The formulation for heat transfer can be expressed as:

$$[C_T^e]\{\dot{\theta}^e\} + [K_T^e]\{\theta^e\} = \{Q^e\} \quad (2)$$

where: $[C_T^e] = \int_V \rho c_p N^T N dV$

$[K_T^e] = \int_V N^T \underline{k} N dV$

$\{Q^e\} = \int_S N^T q dS + \int_V N^T r dV$

$[C_T^e]$ is the heat capacity matrix, $[K_T^e]$ is the conductivity matrix, and $\{Q^e\}$ is the external flux vector. c_p is the specific heat of the material, $\underline{k}$ is the thermal conductivity, q is the surface heat flux, and r is the body heat flux generated by plastic deformation.

A smeared crack model was used to describe the response of the ceramic material when a crack initiates. The crack model does not track individual "macro" cracks. Cracking is assumed to occur when the stress reaches a crack detection criterion surface. This failure surface is a mathematical construction which is a linear relationship between the equivalent pressure stress and the Mises equivalent deviatoric stress. When a crack has been detected its orientation is stored for subsequent calculations. Subsequent cracking at the same point is restricted to being orthogonal to this direction since stress components associated with an open crack are not included in the definition of the failure surface used for detecting additional cracks[14].

3. RESULTS

The elastic modulus is an important property of foam patterns used in investment casting process. When a low density pattern sinks into the slurry, the buoyancy of the pattern causes it to bend and hence produces distortion or possibly cracks in the thin prime coat. The elastic modulus of the foam is required to accurately simulate the possible pattern distortion during shell building process as well as any stress in the shell during pattern removal. Compression testing of the foam was done to determine the elastic modulus. The average measured elastic modulus was 53 MPa.

This data was used to predict foam pattern distortion when it is dipped into the slurry. The deflection of the foam is denoted by "Δ". The density of slurry used in the model was 1.5 g/cm^3. A simple plain-strain finite element model (Figure 3) was

developed in ABAQUS to estimate the distortion of the pattern in the slurry. The dimensions of the foam plate are 127 mm (length) × 6.35 mm (thickness) × 25.4 mm (width). Table 1 lists the material properties of polyurethane and EPS patterns and the calculated pattern deflection. Polyurethane foam has an order of magnitude less deflection during dipping when compared to less rigid EPS foam.

While a higher modulus prevents deflection during shell construction, polyurethane foam may create larger pressures on the shell during foam removal. To understand these effects it is important to know the thermal behavior of the foam. The results of thermal gravimetric analysis (TGA) show that the foam begins to decompose at approximately 260°C regardless of the density, and full decomposition occurred at 600°C (Figure 4).

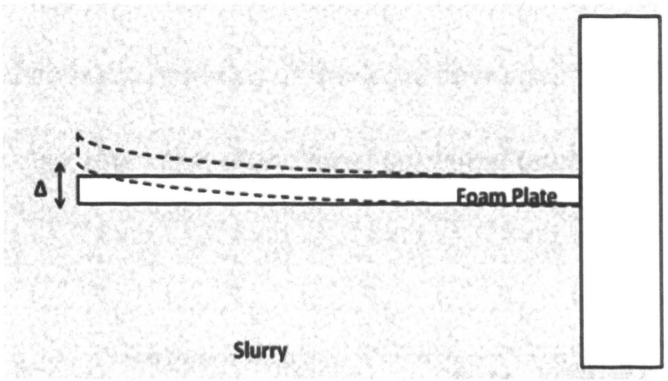

Figure 3. Schematic of the foam deflection model.

Table 1. Foam properties used in model and model results.

Foam	Density, kg/m3	Young's modulus, MPa	Deflection, mm
EPS	26	1.6	70.4
Polyurethane	170	53	2.56

The results from thermal expansion tests show that over the temperature range tested, two distinct regions of differing thermal expansion coefficients can be noticed (Figure 5). At temperatures below 90°C the thermal expansion coefficient is approximately 80 $x10^{-6}$ $°C^{-1}$ while above that temperature the value of the thermal expansion coefficient increases to 400 $x10^{-6}$ $°C^{-1}$. At approximately 155°C the foam stops expanding and begins to soften. At this point the coefficient of thermal expansion becomes slightly negative. The thermal expansion coefficient does not change significantly with changes in density. The maximum dimensional increase of the polyurethane foams that were studied was approximately two percent. An additional thermal expansion test of loaded polyurethane foam was performed for more precise measurement of the effect of temperature on elastic modulus. In this case the elastic modulus at elevated temperatures was estimated from a ratio of applied load to the difference in thermal expansion of the specimens. The results show that above approximately 80°C the elastic modulus of the foam decreases from 53 MPa at a steady rate until it reaches a very low value at the foam softening temperature (155°C).

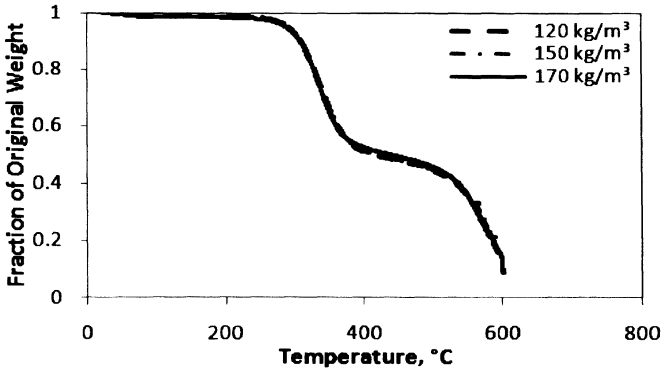

Figure 4. TGA results for three densities of foam in air.

The maximum stress and elastic modulus of the shell was experimentally determined for shells with five and seven layers using three-point bend testing performed at room temperature. Five samples for both types of shells were tested and the failure stress for the five layer shells was lower than the seven layer shells but had a larger elastic modulus (Table 2). The variation in mechanical properties is likely due to a higher percentage of zircon stucco in the five layer shells.

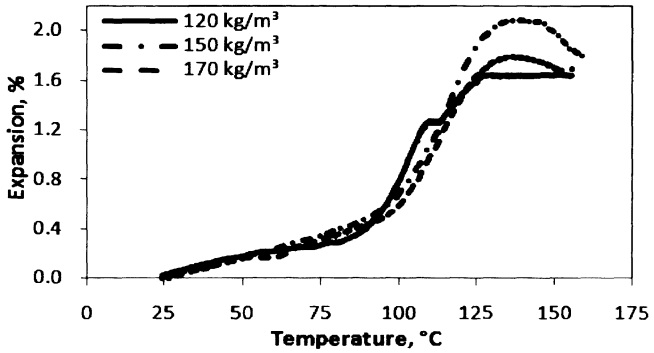

Figure 5. Thermal expansion of polyurethane foam at different densities.

Table 2. Strength and density of shells.

Property	5 Layer Shell	7 Layer Shell
Shell thickness, mm	3.8 ± 0.3	6.4 ± 0.5
Maximum stress, MPa	4.4 ± 0.5	7.2 ± 1.1
Elastic modulus, MPa	3400 ± 500	2000 ± 300
Bulk density, kg/m^3	1900 ± 200	1800 ± 30

The thermo-mechanical properties which were determined for the pattern and the shell were used as input into the model (Table 3). In addition to this experimental data,

the thermal conductivity and specific heat capacity of materials were taken from published data[9, 15-17]. Two types of heating methods (flash fire and continuous heating) were used to remove the foam pattern (Table 4). Due to the shrinkage seen in the thermal expansion tests the foam was assumed to start shrinking when it reaches the foam softening temperature (155°C). The modeling was done for pattern dimensions of 50.8 mm x 63.5 mm x 63.5 mm.

Table 3. Material properties for modeling.

Property	Polyurethane Foam	5 Layer Shell	7 Layer Shell
Density, kg/m^3	170	1800	1800
Poisson's ratio	0	0.24	0.24
Heat capacity, J/gK	1.3	0.65	0.65
Thermal conductivity, W/mK	0.06	1	1
CTE, K^{-1}	$80x10^{-6}$ (20-90°C) $400x10^{-6}$ (90-160°C)	2×10^{-6}	2×10^{-6}

Table 4. Thermal boundary conditions used in the model.

Parameters	Flash Fire	Continuous heating
Heating speed, °C/min	-	3
Oven initial temperature, °C	600	20
Shell surface convection coefficient, W/m^2K	20	20
Shell surface emissivity	0.3	0.3

In the model a linear temperature profile was monitored along the path shown in Figure 6 to compare temperature profiles for different heating methods. Compared to flash firing, the difference between the internal and surface temperatures of the pattern is

not significant in continuous heating. The average temperature of the pattern for flash firing is significantly lower than the average temperature for continuous heating. A lower average temperature means there is less thermal expansion and therefore less pressure on the shell during flash firing.

The distribution of temperature and stress at that moment for the two firing processes is illustrated in Figure 7. The maximum stress in the shell occurs when the boundary temperature between shell and pattern reaches the foam softening temperature. After that, the applied pressure will decrease as a result of foam softening. This critical temperature was experimentally defined from the thermal expansion test. The maximum stress occurs at the internal edges of the shell. Compared to flash firing, continuous heating produces a much higher stress concentration at the internal corner of the shell at a given interface temperature.

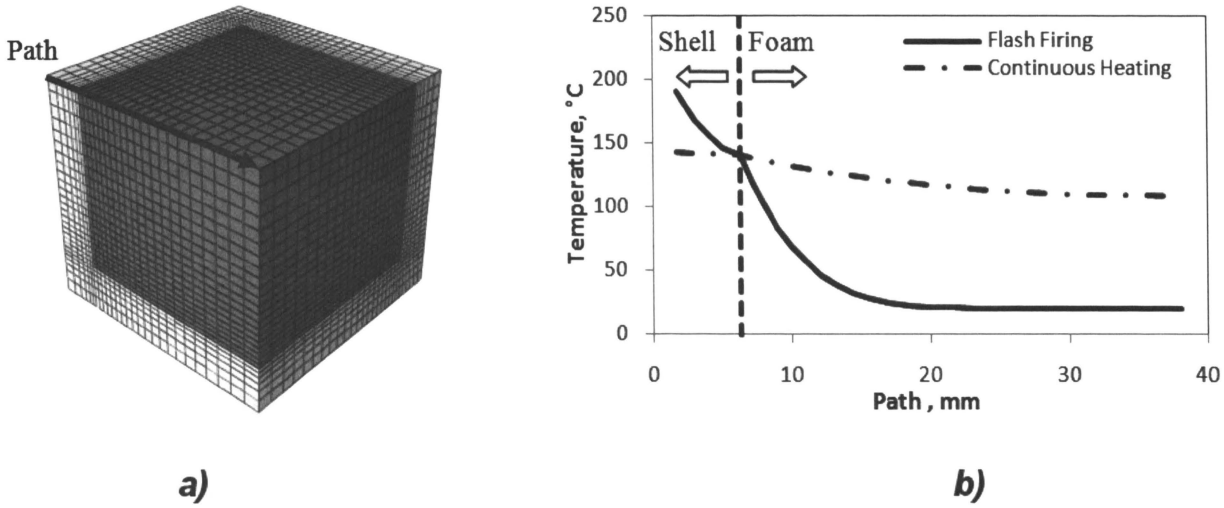

Figure 6. Path (a) and temperature distribution along the path (b) for flash firing and continuous heating at the moment when surface temperature of the pattern increased to the foam decomposition temperature.

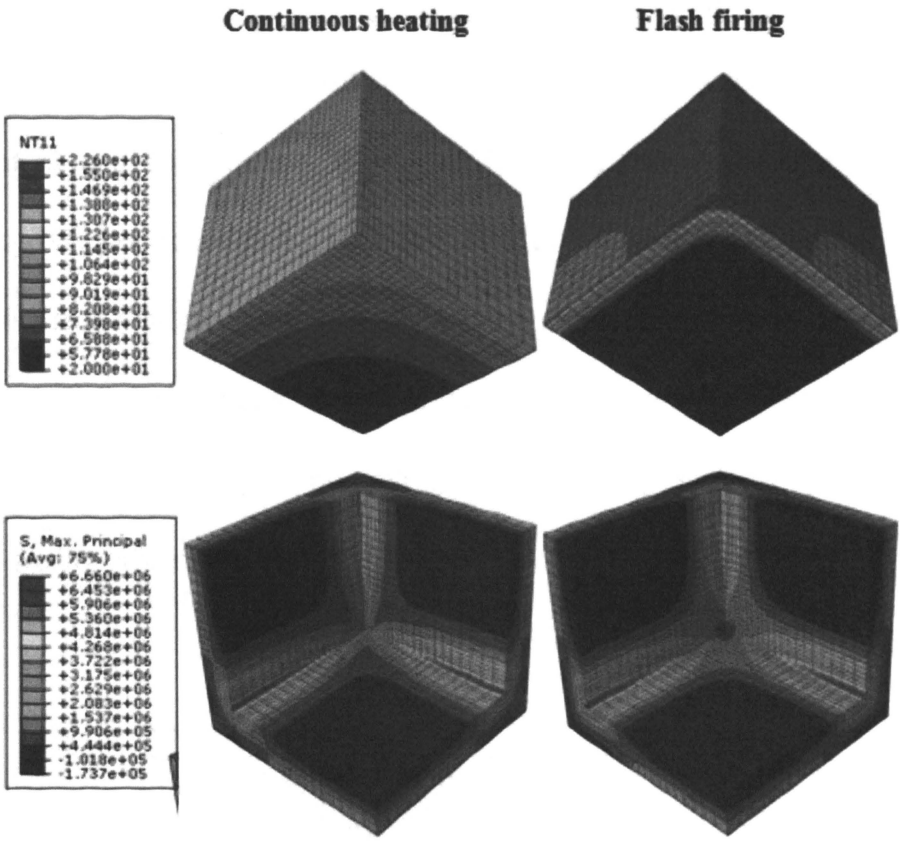

Figure 7. Temperature distribution (a) and maximum principal stress (b) of the shell and pattern at the end of flash firing and continuous heating for 170 kg/m³ foam.

4. DISCUSSION

Crack formation in the shell during rigid foam pattern removal by firing depends on multiple parameters which can be divided into these groups:

Group 1 - *foam properties*, most important of which include elastic modulus, thermal expansion and softening temperature

Group 2 - *shell properties*, most important of which include failure stress, elastic modulus, and shell wall thickness

Group 3 - *firing regime*, continuous heating versus flash firing in high temperature preheated furnace.

In this article, the factors from Group 1 – Group 3 were computationally analyzed. In Group 1 most of the factors are directly affected by the density of the foam. Two extreme cases of foam density, EPS foam (26 kg/m^3) and high density polyurethane foam (170 kg/m^3), were modeled (Figure 8). The low value of elastic modulus in the EPS foam prevents shell cracking for both burnout methods. However, low elastic modulus in the EPS foam causes much more deflection during shell making (Table 2.1). At the same time, the more rigid polyurethane foam creates significantly larger pressure on the shell during pattern removal.

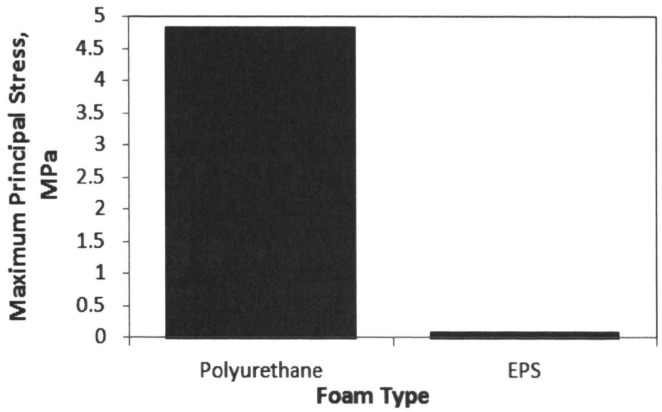

Figure 8. Effect of foam properties on maximal principal stress in shell during pattern flash firing. Lower stress and strain for lower density foams.

In Group 2, the failure stress, elastic modulus, and thickness of the shell are dependent on variables in the shell making process such as slurry viscosity, stucco size and number of coats. It was assumed in a one variable modeling analysis on the effect of shell thickness on cracking tendency that the modulus of the shell does not depend on shell thickness. Results show that thicker shells are less likely to cause shell cracking and increasing shell thickness decreased the maximal principal stress below critical values

(shown by arrow in Figure 9 for non-cracked samples). In low thickness shells, the high stress generates cracks. The maximum principal stress was close to critical for all thicknesses.

In Group 3, the heating rate can affect the amount of material that is expanded, and therefore the amount of stress on the shell (Figure 10). The results show that patterns removed during flash fire were less likely to crack the shell than patterns removed using continuous heating at 3°C/ min.

Some critical situations were modeled according to the properties of laboratory built shells. These cases were experimentally verified using two firing procedures. The comparison of predicted crack formation and experimentally observed cracks (Figure 11) are given in Table 5. The simulation results match well with the experimental results and show that flash firing reduces the chances of shell cracking during pattern removal.

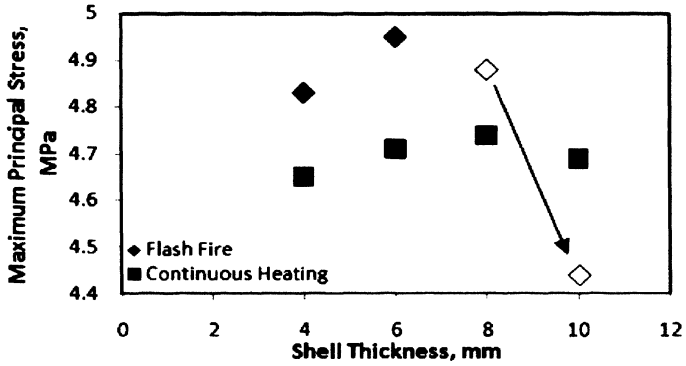

Figure 9. Effect of firing process and shell thickness on maximum principal stress in the shell. Hollow markers designate cases where there was no shell cracking. Indicates less cracking with thicker shells and flash firing.

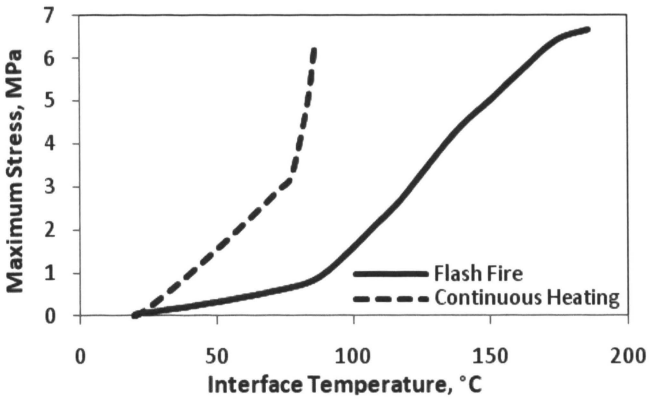

Figure 10. Effect of firing process on maximum principal stress at the point of crack initiation showing significantly higher stresses for continuous heating.

Table 5. Comparison of simulation and experimental results.

Case No	Shell Thickness (mm)	Heating Method	Shell Fail (Simulation)	Shell Fail (Experiment)
1	6.4	Flash firing	No	No
2	6.4	Continuous heating	Yes	Yes
3	3.8	Flash firing	Yes	Yes
4	3.8	Continuous heating	Yes	Yes

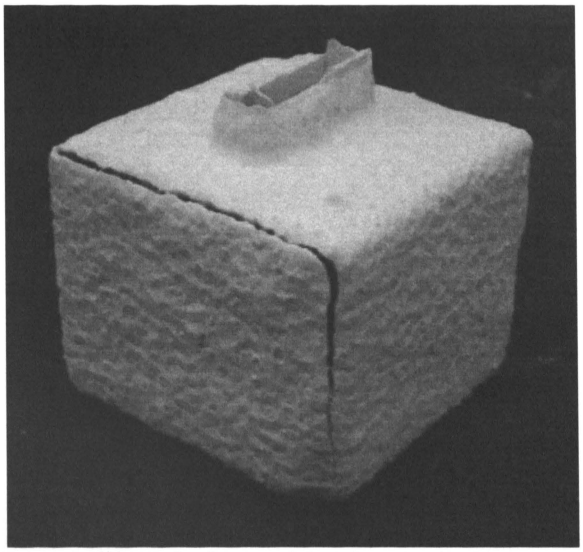

Figure 11. Example of crack formed in the shell during pattern removal.

5. CONCLUSIONS

The mechanism of crack formation in investment casting ceramic shells during rigid polymeric foam pattern removal was analyzed. A model was developed for predicting crack formation in investment casting shells due to pattern expansion. The model takes into consideration the thermal and mechanical properties of the pattern and shell materials to determine the heat transfer and thermal expansion stresses developed in the shell during firing. The model shows that increasing foam density, elastic modulus, and foam softening temperature increase the chance of shell cracking. Increasing the shell strength and thickness decrease the chance of shell cracking. The model accurately predicts the presence of cracking during pattern removal. The results of the model and the experiments demonstrate that patterns should be made with the lower density polyurethane foam in order to prevent shell cracking during pattern removal. It is also recommended that the pattern should be removed using flash firing at 600°C or higher.

ACKNOWLEDGEMENTS

The authors would like to thank U.S. Army Benet Labs for funding this research. The authors wish to recognize the assistance of Darryl Kline for the thermal expansion tests, Hongfang Zhao for TGA analysis, and Tom Towey and Katherine Ramsey for sample preparation.

REFERENCES

1. Foster, G, "Flashfire Dewax for Today's Investment Casting Foundry", Investment Casting Institute 42nd Annual Meeting, pp. 2:1-2:11, Atlanta, Georgia; USA; 25-28 September 1994.

2. Yao, W L; Leu, Ming C, "Analysis of Shell Cracking in Investment Casting with Laser Stereolithography Patterns", Rapid Prototyping Journal, Vol. 5, no. 1, March 1999.

3. Capadona, J A, "Slurry Process Control in Production can "Crack Down" on Shell Cracking", Incast Vol. 4, no. 4 pp. 10-12, April 1991.

4. Guerra, M, Schiefelbein, G W, "Review of Shell Components Shell Characteristics and Properties Refractory Selection for Primary Shell Coat", Investment Casting Institute 42nd Annual Meeting, Atlanta, Georgia; USA; 25-28 September 1994.

5. Arzt, A M, "Optimizing Control of Shell Cracking in Investment Casting", Mod. Cast. Vol. 77, no. 2, pp. 30-33. February 1987.

6. Roberts, W O, "Colloidal Silica", Proceeds of AFS/CMI Symposium on Factors Affecting Shell Cracking, Des Plaines, Illinois, 1987.

7. Schiefelbein, G W, "Ceramic Shell Production for Controlling Shell Cracking", Conference on Factors Affecting Shell Cracking, December 2-3, 1986.

8. Cannell, N, Sabau, A S, "Predicting Pattern Tooling and Casting Dimensions for Investment Casting, Phase II", Final Technical Report, September 2005.

9. Kline, D, Lekakh, S, Mahimkar, C, Richards, V, "Crack Formation in Ceramic Shell During Foam Pattern Firing", Technical and Operating Conference, Chicago, Illinois; USA; December 2009.

10. "Foam Patterns for Investment casting", Modern Casting. Vol. 99, no. 7, pp. p. 46. July 2009.

11. ASTM D1621, "Standard Test Method for Compressive Properties of Rigid Cellular Plastics", ASTM International, 2010.

12. ASTM C1161, "Standard Test Method for Flexural Strength of Advanced Ceramics at Ambient Temperature", ASTM International, 2002.

13. ASTM C20, "Standard Test Methods for Apparent Porosity, Water Absorption, Apparent Specific Gravity, and Bulk Density of Burned Refractory Brick and Shapes by Boiling Water", ASTM International, 2000.

14. ABAQUS Version 6.9. Manual, Dassault Systèmes, 2009.

15. Mahimkar, C, Richards, V L, Lekakh, S N, "High Temperature Thermo-Physical Properties of Ceramic Shell", Investment Casting Institute 57th Annual Conference and Expo, October 10-13, 2010.

16. Sabau, A S, Viswanathan, S, "Thermo-Physical Properties of Zircon and Fused Silica Based Shells for Investment Casting", Transactions of the American Foundry Society, Vol. 112, No. 04-081, pp 649 - 661, 2004.

17. Niknejad, A, Liaghat, G H, Moslemi, N H, Behravesh, AH, "Theoretical and Experimental Studies of the Instantaneous Folding Force of the Polyurethane Foam-Filled Square Honeycombs", Materials and Design. Vol. 32, no. 1, pp. 69-75, January 2011.

II. FOAM PATTERN AGING AND ITS EFFECT ON CRACK FORMATION IN INVESTMENT CASTING CERAMIC SHELLS

W.A. Everhart, S.N. Lekakh, V.L. Richards and J.D. Smith
Department of Materials Science and Engineering

H. Li and K. Chandrashekhara
Department of Mechanical and Aerospace Engineering

H. Zhao and P.S. Nam
Chemistry Department

Missouri University of Science and Technology, Rolla, MO 65409

(Submitted for Publication to the AFS Transactions, August 2011)
(Edited for thesis)

ABSTRACT

The application of rigid plastic foam for large investment casting patterns with complex geometries can improve the dimensional tolerances and the surface quality of the casting. However, these pattern materials promote crack formation in investment casting shells during pattern removal using standard firing procedures. In typical investment casting shell processing, drying stages provide an aging period which can change the compatibility strains of the shell/foam assembly. In order to accurately predict shell cracking occurrence during pattern removal, the aging strain of the pattern must be considered. ASTM standard tests and independently developed experimental methods were combined with finite element modeling to predict stress development in the shell. The model takes into consideration the thermal properties of the pattern and the shell materials to determine the heat transfer to establish a thermal gradient within the materials. This is combined with mechanical properties to determine the thermal expansion stresses developed in the shell during firing. An experimentally measured delay of the thermal expansion of the aged pattern was incorporated in a three-dimensional nonlinear finite element model and used to predict possible crack formation in the shells during pattern removal. The effect of pattern aging on crack formation in the shell was experimentally validated. Recommendations for pattern removal parameters to decrease stress and eliminate crack formation in the shell were formulated.

Key Words: ceramic shell, investment casting, crack, stress modeling, molding

1. INTRODUCTION

The investment casting process is generally used to produce small, thin walled castings with high detail. The process begins with the manufacture of a pattern from an easily shaped, inexpensive material. The most common material for patterns is wax but different types of polymeric foam are also used[1-2]. The pattern is dipped in slurry made of inorganic binder and oxide flour usually containing some combination of fused silica, zircon, alumina, or other ceramic material. Refractory granules referred to as stucco (usually fused silica, zircon or alumina) are then applied to the wet slurry coating. The combination of slurry and stucco makes a single coat which is allowed to dry before subsequent coats are applied. The shell building process generally consists of three different types of layers. Prime coats are designed to provide a better surface finish for the casting and are applied first, usually in one or two coats. Backup coats are designed to add strength to the shell and are applied after any prime coats; four to ten backup coats are applied. The seal coat is designed to seal the stucco of the final backup coat and is applied last[3-7]. The pattern is then removed from the unfired or green shell by melting or decomposition in an autoclave or furnace. Whether done as a part of pattern removal, or as an additional firing process, the ceramic is sintered to increase the strength of the shell such that the pressure of liquid metal will not cause cracks. Liquid metal is then poured into the shell, which is usually preheated, to produce the casting.

Large patterns made from wax often do not have sufficient strength to hold their shape due to their higher weight, especially in situations where the pattern has unsupported extensions, leading to creep[8]. Polymeric foams were considered as pattern materials in investment casting in an attempt to overcome some of the wax deficiencies.

Some of the first foams used were expanded polystyrene (EPS) [9]. This material has much lower density than wax and, despite its lower strength, doesn't suffer from the self loading creep that is common with wax patterns, especially in larger patterns. This becomes especially important to the dimensional stability of the pattern during storage. However, EPS foams are also very buoyant which causes problems when the pattern is initially dipped in the slurry. The forces on the pattern when submerged can be high enough to distort or even break the pattern. EPS foam and wax patterns also show some dimensional change when they are cooled after production. Because of these issues, stronger, higher density polymeric foams are needed. Polyurethane foams fit these requirements well and can be made in complicated shapes with high surface quality and dimensional accuracy[10]. However, polyurethane foams have high coefficients of thermal expansion and high decomposition temperatures which can cause the pattern to expand and break the shell during the pattern removal process[9].

Preliminary aging of EPS patterns to control pattern dimensions has been successfully implemented in lost foam casting[11]. The use of aging to prevent shell cracking is based on the change in pattern dimensions over time, especially at elevated temperatures[12]. The polymeric foam aging mechanism relates to the development of crystallinity. An aged crystalline polymer has two phases: the crystalline phase and the amorphous phase[13]. Preliminary aging of the polymeric foam pattern inside the green shell may increase the ordered domain and crystallinity of the polyurethane pattern during firing leading to volume reduction. Because of this, the effect of the thermal expansion of the polyurethane could be reduced.

The objective of this research was to develop a model to predict the effect of pattern aging on shell cracking. To achieve this goal, the aging properties of the polyurethane foam were experimentally determined along with glass transition temperatures and the Young's modulus of aged foam. Additionally, samples were tested for shell cracking by firing shelled patterns in various conditions. These data were used in a finite element model to predict crack formation during pattern removal.

2. PROCEDURES

Experimental. Polyurethane foam with density of 170 kg/m^3 was tested. Samples were cut from the center of foam blocks with a cross-section of 7000 mm2. Compression testing of the foam was used to determine the elastic modulus after aging at 100°C for 24 hours. Samples had a cross-section of 2580 mm2 and a thickness of 25.4 mm or 50.8 mm (ASTM D1621)[14]. Thermal dilation during foam aging was measured using a laser assisted dilatometer. Foam samples were cut into 50 mm long 18 mm diameter cylinders. Two thin aluminum disks were placed on both ends of the foam and inserted into a quartz glass tube (19 mm diameter) submerged in an oil bath. A small hole was present in the end of the tube to allow oil flow inside for improved heating of the sample. Another quartz tube was placed on the upper aluminum disk. The expansion of the foam sample was monitored through the linear movement of the upper tube using a laser proximity probe with 1 μm precision. The average temperature of the foam samples was collected by averaging the reading of two thermocouples inserted in the oil bath, one of which was inserted in a spare foam sample and the other thermocouple was left exposed to the oil. The heating rate of the foam was approximately 1°C/min. Samples were held at various aging temperatures and times, cooled back to room temperature and

heated aging until softening. Additionally one sample was heated and held at different temperatures in a stepped fashion. Differential scanning calorimetry (DSC) was done on the foam in both the aged and un-aged condition. The samples were stabilized by first heating from room temperature to 180°C in the instrument, then immediately quenched in liquid nitrogen and held for 1 min. The 2mg quenched sample was then tested using DSC (TA instrument DSC Q2000) from -38°C to 210°C at a heating rate of 20°C/min in a nitrogen gas atmosphere.

A simple pattern (50.8 x 63.5 x 63.5 mm) was prepared to test shell cracking during burnout (Figure 1). The slurry consisted of colloidal silica binder (Megasol BI) and fused silica flour (-200 mesh). Slurry viscosity was measured by Brookfield DVII+ Pro Viscometer. All coatings were applied at 800 ± 100 cP viscosity which is equivalent to 19-22 seconds on a #5 Zahn cup. The patterns were submerged in the slurry until completely covered and then removed and suspended over the slurry for approximately 50 seconds. During this time, the pattern was rotated and allowed to drain from different points to promote an even coating. A uniform distribution of stucco was then applied using the rainfall method. This was done by continuously rotating the pattern so that all surfaces were directly impacted by the falling stucco until no more stucco would adhere to the surface. The stucco for the prime coat was granular zircon (-100+200 mesh) and the stucco for the back-up coats was fused silica (-30+50 mesh). The seal coat used no stucco. The samples were dried for at least four hours between coats. Shells were fabricated with one prime coat, either three or five backup and one seal coat. The samples with three backup coats had five total layers (3.8 mm average thickness) and the samples with five backup coats had seven total layers (6.4 mm average thickness). After

the seal coat was applied the samples dried for another 24 hours. Half of the patterns were then aged. After sample preparation the shells were fired in electrical resistance box furnace using flash firing in a furnace preheated to 600°C.

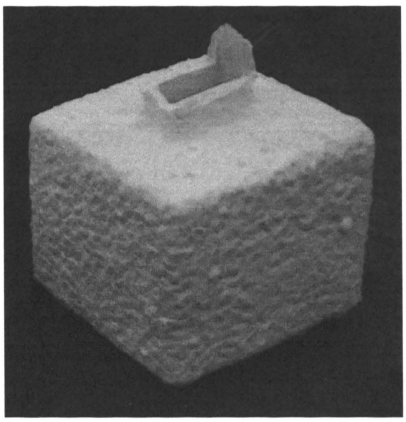

Figure 1. Shell built around foam pattern: 50.8 x 63.5 x 63.5 mm.

The maximum stress at rupture and elastic modulus of the five and seven layer shells were determined using three point bend testing of green shells performed at room temperature according to ASTM C1161[15]. The tip of the testing fixture had a radius of three mm. The bulk density of the shells was measured using Archimedes method in distilled water according ASTM C20 using approximately 10 g samples[16].

Modeling. A nonlinear coupled finite element model was developed to study the crack formation in the shell during pattern removal. The model accounts for both mechanical and thermal loadings and assumes a fixed interface between the pattern and shell. It is capable of simulating the complete detail of pattern and shell behavior during the firing process. To reduce computational time, one quarter of the pattern surrounded by shell has been modeled and symmetric boundary conditions are applied at the cut

planes. An eight-node brick element is used to mesh the model. To mesh the pattern, all edges are initially seeded by numbers. In order to obtain higher result accuracy and save computational cost, additional seeds and biased seeds are used in critical regions and fewer seeds in regions that are less of interest, and hex mesh shape and structured mesh technique are used. The mesh of the finite element model for both the shell and foam pattern is shown in Figure 2. Finer mesh is used near the corner of ceramic shell. 19,683 brick elements were used for the model. The contact properties between the pattern and shell are defined as fixed in order to simulate the actual experimental process.

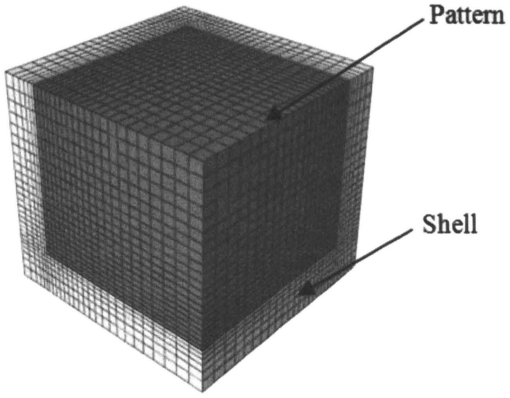

Figure 2. Mesh of finite element model for the foam pattern and ceramic shell.

The formulation for the transient mechanical analysis can be written as:

$$[M^e]\{\ddot{U}^e\} + [K^e]\{U^e\} = \{F^e\} + \{F_T^e\} \qquad (1)$$

where: $[M^e] = \int_V \rho[N]^T[N]dV$

$[K^e] = \int_V [B]^T[C][B]dV$

$\{U^e\} = \{u, v, w\}^T$

$[M^e]$ is the mass matrix, $[K^e]$ is the stiffness matrix, $\{F^e\}$ and $\{F_T^e\}$ are mechanical and thermal loadings, N is shape function, B is strain-displacement function, C is elasticity matrix, ρ is the density, and $\{u, v, w\}^T$ are displacement components in a rectangular Cartesian coordinate system.

The formulation for heat transfer can be expressed as:

$$[C_T^e]\{\dot{\theta}^e\} + [K_T^e]\{\theta^e\} = \{Q^e\} \tag{2}$$

where: $[C_T^e] = \int_V \rho c_p N^T N dV$

$[K_T^e] = \int_V N^T \underline{k} N dV$

$\{Q^e\} = \int_S N^T q dS + \int_V N^T r dV$

$[C_T^e]$ is the heat capacity matrix, $[K_T^e]$ is the conductivity matrix, and $\{Q^e\}$ is the external flux vector. c_p is the specific heat of the material, $\underline{k}$ is the thermal conductivity, q is the surface heat flux, and r is the body heat flux generated by plastic deformation.

A smeared crack model was used to describe the response of the ceramic material when a crack initiates. The crack model does not track individual "macro" cracks. Cracking is assumed to occur when the stress reaches a crack detection criterion surface. This failure surface is mathematical construction which is a linear relationship between the equivalent pressure stress and the von Mises equivalent deviatoric stress. When a crack has been detected its orientation is stored for subsequent calculations. Subsequent cracking at the same point is restricted to being orthogonal to this direction since stress components associated with an open crack are not included in the definition of the failure surface used for detecting additional cracks[17].

3. RESULTS

Experimental. The effect of time and temperature on foam aging is important when this behavior benefits the process by reducing shell cracking. Appropriate aging times and temperatures can be vital when applying this method to industry. A preliminary study on the effect of aging was done with a sample that was heated and held at various temperatures in a stepping fashion (Figure 3). This test shows that the aging rate significantly increases at temperatures above approximately 80°C.

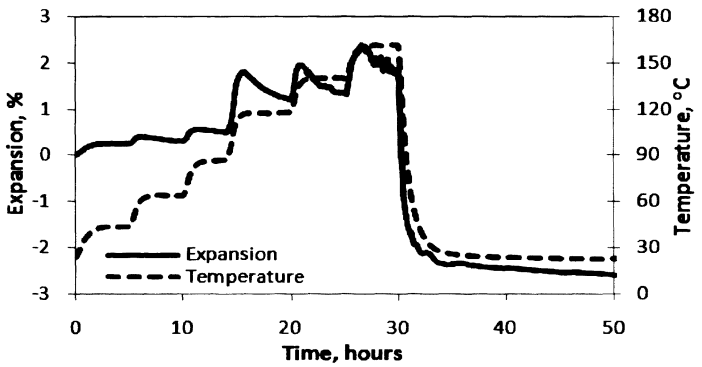

Figure 3. Thermal expansion of the stepped aging sample showing increased shrinkage above 80°C.

Separate samples were then aged at various temperatures for 24 hours to determine the effect of aging temperature on the maximum shrinkage, and expansion after aging (Figure 4b). These results suggest that shrinkage from aging increases at temperatures above 60°C. Temperatures above 100°C were not tested because these temperatures are high enough to cause shell cracking from pattern expansion. Samples were also aged for various amounts of time at 100°C to determine the effect of aging time

on the amount of shrinkage (Figure 4). The results show that after 24 hours the amount of shrinkage does not significantly increase until the aging time is longer than 48 hours.

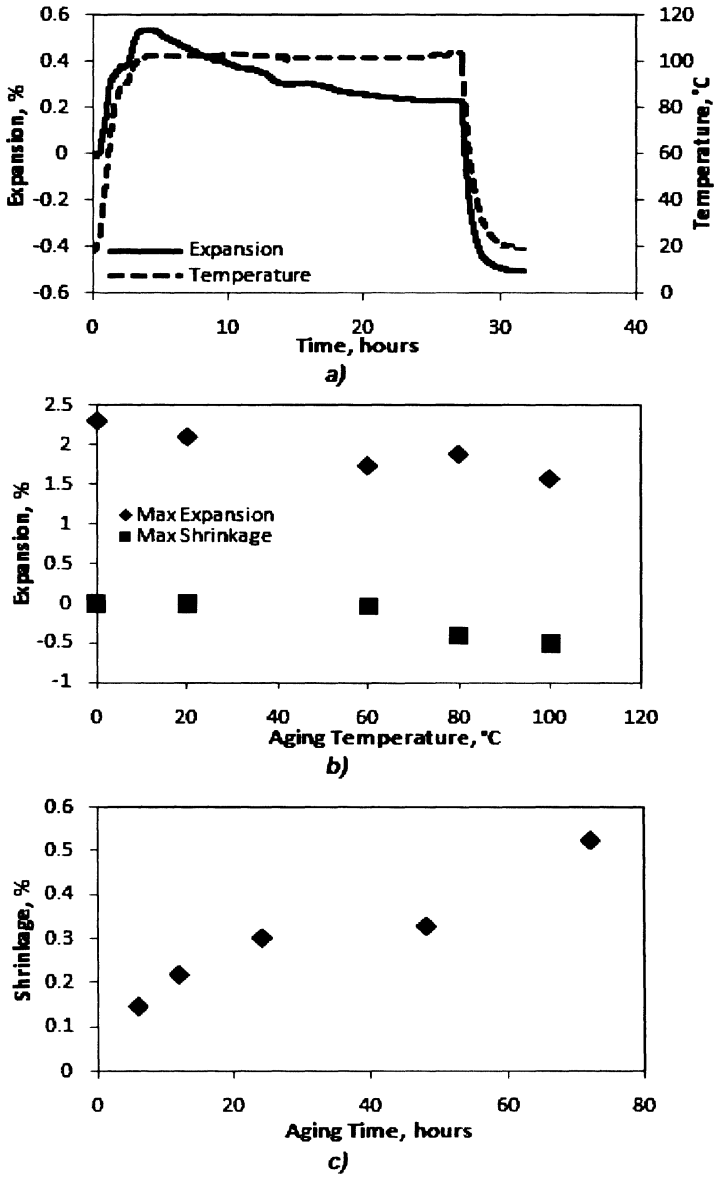

Figure 4. Example of an aging test of polyurethane foam at 100°C (a), maximum expansion/shrinkage of polyurethane foam after 24 hours aging at various temperatures (b) and final shrinkage of polyurethane foam after aging for various amounts of time at 100°C (c).

The CTE of an un-aged sample of polyurethane foam at temperatures below 90°C is approximately 80 $x10^{-6}$ $°C^{-1}$ while above that temperature the CTE increases to 400 $x10^{-6}$ $°C^{-1}$. At approximately 155°C the foam stops expanding and begins to soften. At this point the CTE becomes slightly negative. Aged samples showed similar CTE behavior and foam softening temperature, but because the sample had contracted during aging and did not return to its original size until it had been heated to approximately 80°C, the net expansion of the aged foam relative to a shell mold of fixed dimension was less (Figure 5).

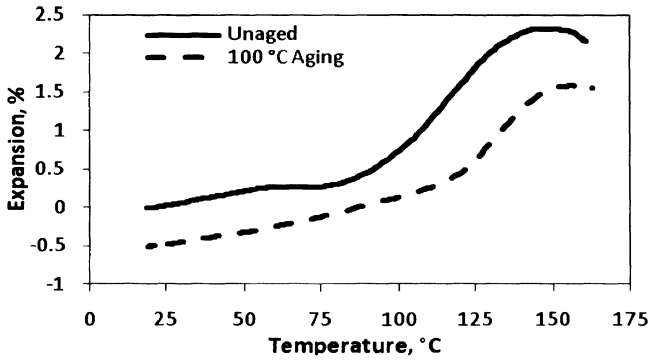

Figure 5. Comparison of the thermal expansion of an aged and un-aged sample.

To study the physico-chemical nature of polyurethane foam aging, DSC testing of the foam was performed. Results showed two endothermic peaks, indicated by changes in slope, one at approximately 60°C and another at approximately 140°C (Figure 6). The 60°C peak is a glass transition temperature and matches well with the transition in CTE. The 140°C peak matches the foam softening temperature and is associated with the break down of the crystalline structure.

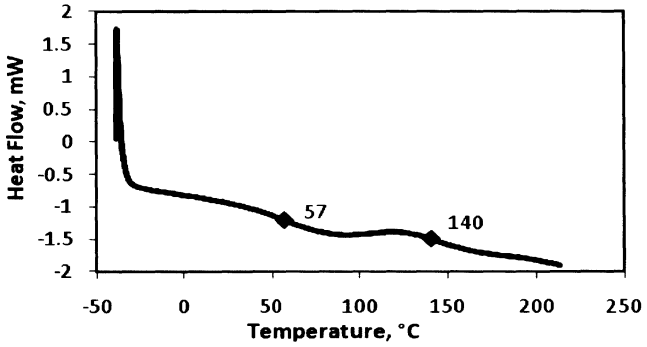

Figure 6. Example DSC results of polyurethane foam showing the endothermic peaks.

The elastic modulus is an important property of foam patterns used for investment casting because of its impact on shell cracking. The effect of aging on the elastic modulus of the foam was determined by comparing the results of compression testing of aged and un-aged samples at room temperature. The average elastic modulus of un-aged samples was 53 MPa and the average modulus of samples that were aged at 100°C for 24 hours was 52 MPa. This implies that aging has no significant effect on the room temperature mechanical properties of foam pattern. Temperature dependent values of the elastic modulus of the foam are required to accurately simulate stress in the shell during pattern removal. These values were determined using the known[18, 19] tendency of the elastic modulus to degrade above the glass transition temperature. In the model the elastic modulus begins to degrade at 80°C until it is near zero at the foam softening temperature.

The maximum failure stress and elastic modulus of the shell were experimentally determined for shells with five and seven layers using three-point bend testing performed at room temperature. Five samples for both types of shells were tested and the calculated values are included in Table 1. The failure stress for the five layer shells was lower than the seven layer shells while the five layer shells had a higher elastic modulus. The

variation in mechanical properties is likely due to a higher percentage of zircon stucco in the five layer shells.

Table 1. Strength and density of shells.

Property	5 Layer Shell	7 Layer Shell
Shell thickness, mm	3.8 ± 0.3	6.4 ± 0.5
Maximum stress, MPa	4.4 ± 0.5	7.2 ± 1.1
Elastic modulus, MPa	3400 ± 500	2000 ± 300
Bulk density, kg/m^3	1900 ± 200	1800 ± 30

Modeling. The experimentally verified thermo-mechanical properties for the pattern and the shell were used as input into the model (Table 2). The foam is assumed to decompose when it reaches a temperature of 155°C. Instead of modeling the actual shrinkage that occurs during aging, the CTE from room temperature to 80°C for aged samples is set to zero in the simulation. A zero CTE prevents stress development in the shell by approximating the gap formed by aging and the subsequent free expansion of the pattern until the pattern expands to fill the gap (Figure 7). In addition to the experimental data in Table 1, thermal conductivity and specific heat capacity data were used[9, 20-22]. The thermal boundary conditions for flash firing at 600°C used in the simulations are shown in Table 3. Modeling was completed for aged (100°C for 24 hours) and un-aged samples with pattern dimensions of 50.8 x 63.5 x 63.5 mm.

Table 2. Material properties for modeling[9, 20-22].

Property	Polyurethane Foam	5 Layer Shell	7 Layer Shell
Density, kg/m^3	170	1800	1800
Poisson's ratio	0	0.24	0.24
Heat capacity, J/gK	1.3	0.65	0.65
Thermal conductivity, W/mK	0.06	1	1
CTE, K^{-1}	See Figure 7	2×10^{-6}	2×10^{-6}

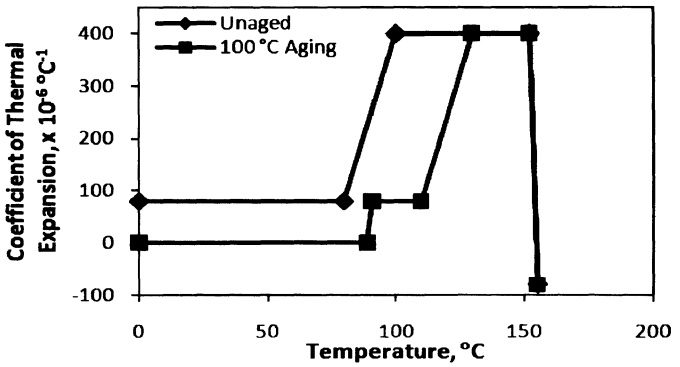

Figure 7. CTEs used in simulation for aged and un-aged samples. This shows the assumptions made for the aged sample to approximate aging shrinkage in the model.

Table 3. Thermal boundary conditions.

Parameters	Flash Fire
Oven initial temperature	600°C
Shell surface convection coefficient	20 W/m^2K
Emissivity of the shell surface	0.3

An example of the modeling results for flash fire at 600°C for aged and un-aged patterns with shell thickness of 6.4 mm is included as Figure 8. The maximum stress in the shell occurs when the boundary temperature between shell and pattern reaches the foam softening temperature. At that temperature, the applied pressure begins to decrease

as a result of foam softening. This critical temperature was experimentally defined from the thermal expansion results. The maximum stress for both aged and un-aged samples occurs at the internal edges of the shell (Figure 8). Compared to aged, an un-aged sample produces a much higher stress concentration in the shell.

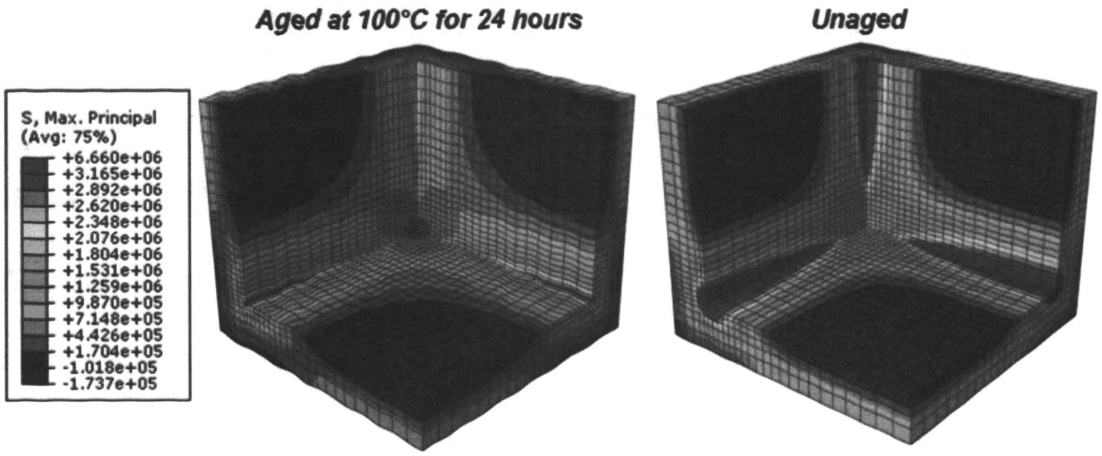

Figure 8. Maximum principal stress distribution of the shell at the end of flash firing and for aged and un-aged foam patterns.

4. DISCUSSION

Crack formation in the shell during rigid foam pattern removal by heat treatment depends on multiple parameters which can be divided into the following groups:

Group 1 - *foam properties*, most important of which include elastic modulus, thermal expansion, softening temperature and aging

Group 2 - *shell properties*, most important of which include failure stress, elastic modulus, and shell wall thickness

Group 3 - *firing regime*, continuous heating versus flash firing in high temperature preheated furnace.

The effect of aging after shell building and before pattern removal on polyurethane foam properties and shell cracking during pattern removal was investigated. Longer aging times were shown to increase the amount of shrinkage, especially for times less than 24 hours. After approximately 20 hours the shrinkage for a pattern aged at 100°C subsides due to nearing completion of the transformation from an amorphous structure to a crystalline structure (Figure 4a). When aging temperature is above the glass transition temperature indicated by DSC (approximately 60°C) the amount of shrinkage increases from zero to 0.5% (Figure 4b) supporting the idea that the transformation of the polyurethane foam from amorphous to crystalline is the aging mechanism. Activation energy for aging was determined from the shrinkage in Figure 3. The activation energy was approximately 600 J/mol when aging was below 80°C and 1800 J/mol when above 80°C. Foam aging was not found to increase or decrease the elastic modulus of the polyurethane foam.

During pattern removal the strain in the pattern consists of aging strain, thermal strain and elastic strain and the strain in the shell consists of thermal strain and elastic strain. The small amount of shrinkage caused by aging induces a negative strain in the pattern. This negative strain reduces the overall strain in the pattern and shell at their interface thus lowering the stress developed in the shell (Figure 9).

This concept was applied to a shell cracking model to show the effect of aging on the stress developed in the shell during pattern removal and specific cases were experimentally verified in the laboratory shell cracking test (Figure 10). The comparison of experimental results and prediction of crack formation in the model are given in Table 4, indicating that modeling is consistent with experimental results. Aging the patterns

significantly reduced the stress in the shell during pattern removal. Aging prevented cracking of the 3.8 mm thick shells and lowered stress development in the 6.4 mm shells (Figure 9).

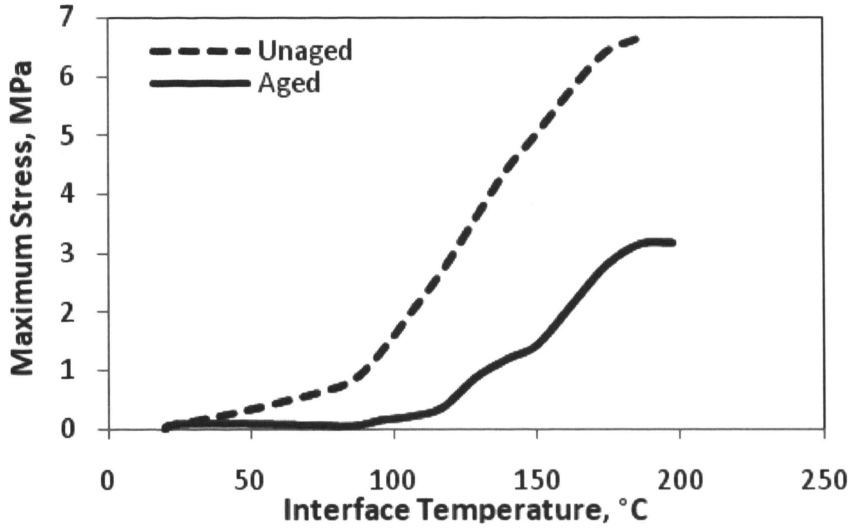

Figure 9. Comparison of stress development in the 6.4 mm thick shell for aged and un-aged foam patterns showing significantly higher stress in un-aged patterns.

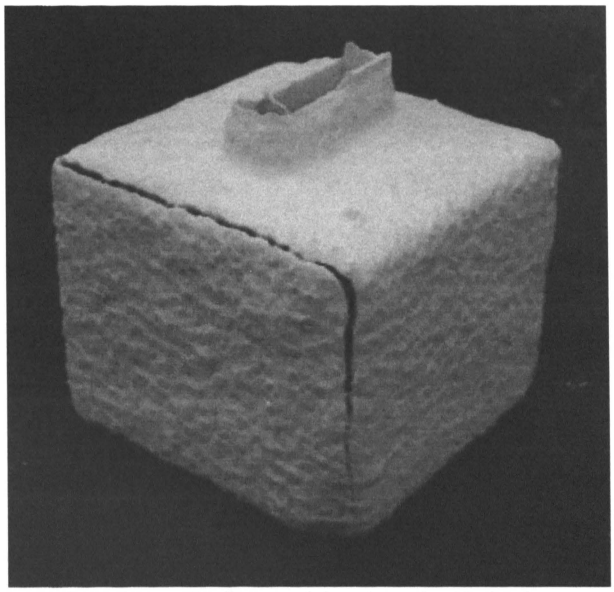

Figure 10. Example of crack formed in the shell during pattern removal.

Table 4. Comparison of simulation and experimental results.

Case No	Shell Thickness (mm)	Aging	Shell Fail (Simulation)	Shell Fail (Experiment)
1	6.4	Not Aged	No	No
2	3.8	Not Aged	Yes	Yes
3	6.4	Aged 100 °C	No	No
4	3.8	Aged 100 °C	No	No

5. CONCLUSIONS

Aging reduces the stress in the shell by producing shrinkage which lowers the compatibility strain on heating and its consequent elastic stress development. A model was developed for predicting crack formation in investment casting shells due to pattern expansion. The model accurately predicts the presence of cracking during pattern removal for un-aged patterns with five layer shells. The results of the model and the experiments demonstrate that aging patterns can be an effective way to prevent shell cracking during pattern removal. To effectively prevent shell cracking it is recommended that aging be done above the glass transition temperature (60°C) for at least 24 hours.

ACKNOWLEDGMENTS

The authors would like to thank US Army ARDEC - Benet Labs for funding this research. The authors wish to recognize the assistance of Darryl Kline for the thermal expansion tests, and Tom Towey and Katherine Ramsey for sample preparation.

REFERENCES

1. Foster, G, "Flashfire Dewax for Today's Investment Casting Foundry", Investment Casting Institute 42nd Annual Meeting, pp. 2:1-2:11, Atlanta, Georgia; USA; 25-28 September 1994.

2. Yao, W L, Leu, M C, "Analysis of Shell Cracking in Investment Casting with Laser Stereolithography Patterns", Rapid Prototyping Journal, Vol. 5, no. 1, March 1999.

3. Capadona, J A, "Slurry Process Control in Production can "Crack Down" on Shell Cracking", Incast Vol. 4, no. 4, pp. 10-12, April 1991.

4. Guerra, M, Schiefelbein, G W, "Review of Shell Components, Shell Characteristics and Properties: Refractory Selection for Primary Shell Coat", Investment Casting Institute 42nd Annual Meeting, Atlanta, Georgia; USA; 25-28 September 1994.

5. Arzt, A M, "Optimizing Control of Shell Cracking in Investment Casting", Mod. Cast. Vol. 77, no. 2, pp. 30-33. February 1987.

6. Roberts, W O, "Shell Cracking – a Complete and Detailed Compilation of Papers, Case Histories, and Discussions Presented at the AFS/CMI Symposium "Factors Affecting Shell Cracking", "Colloidal Silica", American Foundrymen's Society, Publications Department, Golf & Wolf Roads, Des Plaines, IA, 1987.

7. Schiefelbein, G W, "Ceramic Shell Production for Controlling Shell Cracking", Conference on Factors Affecting Shell Cracking, December 2-3, 1986.

8. Cannell, N, Sabau, A S, "Predicting Pattern Tooling and Casting Dimensions for Investment Casting, Phase II", Final technical report, September 2005.

9. Kline, D, Lekakh, S, Mahimkar, C, Richards, V, "Crack Formation in Ceramic Shell During Foam Pattern Firing", Technical and Operating Conference, Chicago, Illinois; USA; December 2009.

10. "Foam Patterns for Investment casting", Modern Casting, Vol. 99, no. 7, pp. 46, July 2009.

11. Smith, B V, Biederman, S, "Examining Lost Foam's 'White side'", Modern casting, Vol. 90, no. 8, August 2000.

12. Li, X ; Cao, H, Zhang, Y, "Structures and Physical Properties of Rigid Polyurethane Foams with Water as the Sole Blowing Agent", Science in China. Series B, Chemistry, Vol. 49, no. 4, pp. 363-370, 2006.

13. Ho, T, Wynne, K J, "A New Fluorinated Polyurethane: Polymerization, Characterization, and Mechanical Properties", Macromolecules, pp.3521-3527, 1992.

14. ASTM D1621, "Standard Test Method for Compressive Properties of Rigid Cellular Plastics", ASTM International, 2010.

15. ASTM C1161, "Standard Test Method for Flexural Strength of Advanced Ceramics at Ambient Temperature", ASTM International, 2002.

16. ASTM C20, "Standard Test Methods for Apparent Porosity, Water Absorption, Apparent Specific Gravity, and Bulk Density of Burned Refractory Brick and Shapes by Boiling Water", ASTM International, 2000.

17. ABAQUS Version 6.9. Manual, Dassault Systèmes, 2009.

18. Kinyanjui, J., "Thermally Induced Changes in the Chemical and Mechanical Properties of Epoxy Foam", Journal of Cellular Plastics. Vol. 46, no. 6, pp. 531-549, 2010.

19. Batallas, B., Yih, H., Singh, P., "Determining the Performance of Polyurethane Foam Pipe Insulation for High Temperature Service", Northern Area Western Conference, Calgary, Alberta, CA, 2006

20. C. Mahimkar, V. L. Richards, S.N. Lekakh, "High Temperature Thermo-physical Properties of Ceramic Shell", Missouri University of Science & Technology, ICI, 2009

21. Sabau, A S, Viswanathan, S, "Thermo-physical Properties of Zircon and Fused Silica Based Shells for Investment Casting", Transactions of the American Foundry Society, Vol. 112, No. 04-081, pp 649 - 661, 2004.

22. Niknejad, A, Liaghat, GH, Moslemi, N H, Behravesh, AH, "Theoretical and Experimental Studies of the Instantaneous Folding Force of the Polyurethane Foam-filled Square Honeycombs", Materials and Design. Vol. 32, no. 1, pp. 69-75, January 2011.

III. CORNER STRENGTH OF INVESTMENT CASTING SHELLS

W.A. Everhart, S.N. Lekakh and V.L. Richards
Department of Materials Science and Engineering

J. Chen, H. Li and K. Chandrashekhara
Department of Mechanical and Aerospace Engineering

Missouri University of Science and Technology, Rolla, MO 65409

(Submitted for Publication to the Journal of Engineering Fracture Mechanics, August 2011)
(Edited for thesis)

ABSTRACT

During the investment casting process, particularly pattern removal and pouring steel into the free standing ceramic shell, the shell is subjected to high internal pressure and thermal stress. Most testing methods investigate the properties of the ceramic shell in flat regions while cracks typically form in sharp corners and edge regions. The corners and edge regions have different structure and thickness when compared to flat regions and experience large mechanical stress during processing. In this study, experimental methods were combined with finite element modeling to predict failure stress in internal corner regions of the shell. The model takes into consideration the mechanical properties of the ceramic shell to determine the stress developed during loading. The effect of shell porosity on stress concentration in sharp corners was evaluated. A general equation was developed to predict the force necessary for crack formation in the shell based on various geometric variables. The results from the model were experimentally verified and the failure stress of flat and corner regions of the shell were compared in order to develop an improved equation.

Key Words: Investment casting, ceramic shell, stress, crack

1. INTRODUCTION

The investment casting process is generally used to produce small, thin walled castings with high detail. The process starts with the manufacture of a pattern. The most common material for patterns is wax but different types of polymeric foam and laser stereolithography patterns are also used[1-2]. The pattern is dipped in slurry made of ceramic binder and flour usually containing some combination of fused silica, zircon, alumina, or other ceramic material. Refractory granules referred to as stucco are then applied to the wet slurry coating. The combination of slurry and stucco makes a single coat which is allowed to dry before the next coat is applied. The shell building process generally consists of one or two prime coats, designed to provide a better surface finish for the casting, four to ten back up coats, designed to add strength to the shell, and a seal coat, designed to seal the stucco of the final backup coat[3, 4]. The structure in corners of the shell can be different from flat regions due to the placement of the stucco. Variation of the structure can cause these regions of the shell to break under smaller loads[5]. The pattern is then removed from the shell by melting or decomposition in an autoclave or furnace. Whether done as a part of pattern removal, or as an additional firing process, the ceramic is sintered to increase the strength of the shell enough to hold the pressure of liquid metal. Liquid metal is then poured into the free standing shell, which is usually preheated.

Many new pattern materials, such as polymeric foams, have greater coefficients of thermal expansion than wax which can increase the chance of shell cracking during pattern removal[6]. Due to the majority of these cracks forming along the edges and in the corners of the shell, the properties of these areas are of interest. Investment casting shells

often have complex geometry with sharp internal corners and edges which also initiate stress concentration in addition to pores structure. Work has been done to determine the strength of these areas of the investment shell compared to flat regions[7]. A test method has been developed using a wedge design. Along with this test method, an equation to determine the failure stress (σ, MPa) in the corner region of the wedge was developed:

$$\sigma = \frac{12.2(\sin\theta\cos\theta Fd)}{WT^2} \quad (1)$$

where: θ is the angle from vertical of the splitter used during the wedge test, d is length, W is width, and T is the thickness of the sample in mm and F is the failure force in N. Eq. 1 follows from simplified stress analysis and does not consider the angle of the sample or the radius of the corner of the sample. It is well known that the radius of the corner is important due to its effect as a stress concentrator[8].

Investment casting shells have large porosity due to the stuccoing process. Recently published experimental strength and porosity data of various porous ceramics were reviewed and these data were compared with those calculated from both the minimum contact solid area (MCA) and the pore stress concentration effect (SCE) models[9]. According to the MCA model, the mechanical strength of fully dense ceramic decreases exponentially with increasing volume fraction porosity (P):

$$\sigma = \sigma_0 exp(-bP) \quad (2)$$

where: b is an empirical parameter related to the minimum solid area and dependent on the pore structure.

According to the SCE model, the resulting fracture strength-porosity relationship for all ceramic materials can be given by a power equation of the form:

$$\sigma = \sigma_0(1-P)^n \quad (3)$$

where: η is related directly to the pore structure (shape and orientation of the pores with respect to the stress axis) and the Poisson's ratio of the material.

It was observed that the MCA model better matched the experimental results of ceramics in the low volume fraction porosity range ($P < 0.25$) range, whereas larger volume fraction porosity ceramics ($P > 0.35$) are more accurately modeled by the SCE model[8]. Because investment casting shells have between 0.2 and 0.3 volume fraction porosity[9, 10], both models could be used to predict the flexural breaking stress in flat regions typically obtained from three or four-points bend tests[11]. Stress concentration at both the corner radius of the investment shell and its internal pores could interact, affecting the overall stress intensity in the shell.

The objective of this research was to develop a test procedure to determine the properties of investment casting shells in flat and edge regions and to investigate the effect of shell geometry on the force required to break the shell. Finite element modeling, experimental wedge testing and microstructural analysis were used to determine the effect of shell geometry and structure on crack formation in shell corners.

2. PROCEDURES

Experimental. A wedge pattern was designed to test shell strength along the edge (Figure 1b). Specimens were made from triangular prism shaped patterns 152 mm tall, 76 mm wide with a 15° angle from vertical (30° included angle) with variation from 0.5 mm to 5.0 mm corner radius (Figure 1a). Several wedge and flat specimens for three-point bend testing were made from the triangular prisms. Flat specimens were also tested with an artificial stress concentrator approximately 1.0 mm depth and 0.4 mm wide

(Figure 1c) that was cut by a diamond blade. Five specimens for each condition were tested.

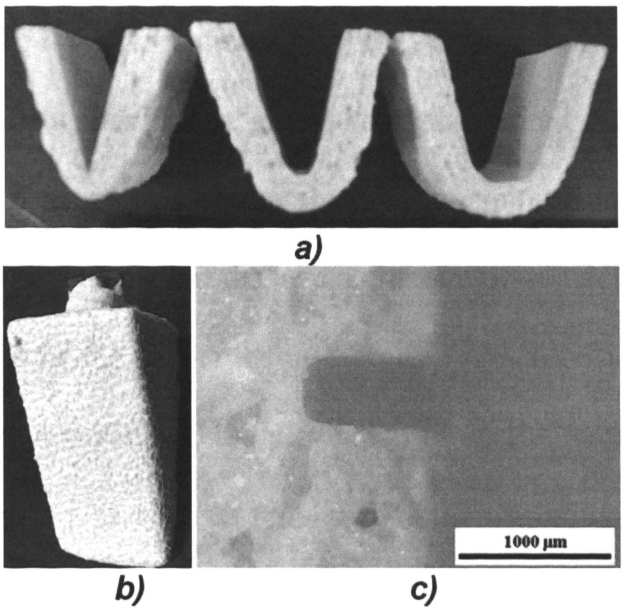

Figure 1. Wedge specimens (a), shell built around foam pattern (b) and the artificial stress concentrator used in flat specimens (c).

The slurry was made of colloidal silica binder (Megasol BI) and fused silica flour (-200 mesh). Slurry viscosity was measured by Brookfield DVII+ Pro Viscometer. All coatings were applied at 800 ± 100 cP viscosity which is equivalent to 19-22 seconds on a #5 Zahn cup. The patterns were submerged in the slurry until completely covered and then removed and suspended over the slurry for approximately 50 seconds allowing for excess slurry to drain. During this time, the pattern was rotated and allowed to drain from different points to promote an even coating. A uniform distribution of stucco was then applied using the rainfall method by continuously rotating the pattern so that all surfaces were directly impacted by the falling stucco until no more stucco would adhere

to the surface. The stucco for the prime coat was granular zircon (-100+200 mesh) and the stucco for the back-up coats was fused silica (-30+50 mesh). The seal coat used no stucco. The samples were dried for at least four hours between coats. The shells were fabricated with one prime coat, five backup coats, and one seal coat. After the seal coat was applied the samples dried for another 24 hours. Acetone was used to remove the EPS foam patterns without altering the "green" strength (unfired strength) of the shell.

The mechanical properties of the shell were explored in the green and fired conditions (1000°C for 1 hour) for flat and corner regions with variations in corner geometry. Assessment of the properties in the green condition is important for stress analysis during pattern removal and the prevention of shell cracking. Properties in the fired condition are important to determine shell integrity during steel pouring. The maximum stress at rupture and elastic modulus of the flat specimens were determined using three-point bend testing of shells performed at room temperature according to ASTM C1161[12]. The tip of the testing fixture had a radius of 3.0 mm. The porosity of the shells was measured using two methods; Archimedes method (ASTM C20[13]) and helium picnometry.

Modeling. A static displacement controlled finite element model has been developed in this work to determine the stress in the ceramic shell at edges where cracks often initiate and propagate. The finite element model is capable of finding the applied force on the wedge and the stress on the ceramic shell. To save computational cost, one quarter of the wedge and ceramic shell has been modeled and symmetric boundary conditions are applied (Figure 2b). The model was cut along the x-z plane and the y-z plane. Shells with different combinations of width (w), length (d), radius (r), and shell

angle (α) were modeled. The loading wedge used in the model had an angle θ of 22.5° from vertical (Figure 2a). In addition, the three-bend point test was modeled for specimens with and without an artificial stress concentrator (Figure 2).

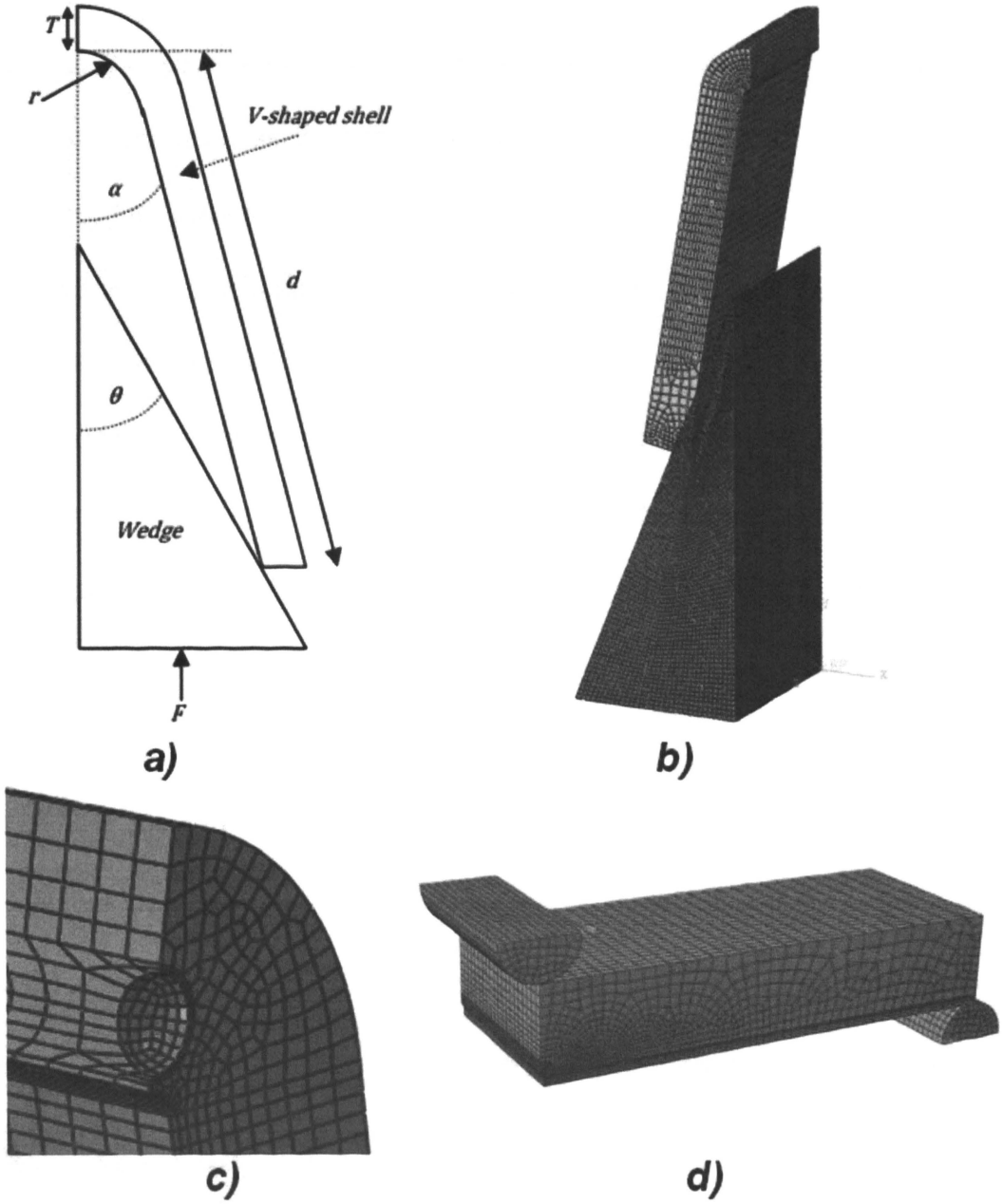

Figure 2. Schematic of the wedge test (a), mesh of finite element model of wedge specimen without (b) and with pore (c), mesh of three-point bend test flat specimen with notch (d).

ABAQUS[14] version 6.9 was used to conduct all the simulation work. Denser mesh is used in critical regions, such as the internal corner of the ceramic shell and the contact surface between the shell and the wedge. 12,600 8-node linear brick elements have been used for the ceramic shell. The wedge is assumed to be a rigid body, and 12,142 4-node 3-D bilinear rigid quadrilateral elements are used. To mesh the wedge test 3D model, all edges are initially seeded by numbers. In order to obtain higher result accuracy and save computational cost, additional seeds and biased seeds are used in critical regions and fewer seeds in regions that are less of interest, and hex mesh shape and structured mesh technique are used. The finite element meshes for the V-shaped ceramic shell with and without a spherical pore are shown in Figure 2a. The contact properties between the shell and the wedge are defined to allow slip in order to simulate the actual experimental process. Maximum principal stress is identified to monitor the actual stress variations in the shell because the shell is a brittle material with high porosity. The formulation for static displacement controlled mechanical analysis can be written as:

$$[K^e]\{U^e\} = \{F^e\} \tag{4}$$

where: $[K^e] = \int_V [B]^T [C][B] dV$

$\{U^e\} = \{u, v, w\}^T$

$[K^e]$ is the stiffness matrix, $\{F^e\}$ is mechanical loadings, B is the strain-displacement function, C is the elasticity matrix, and $\{u, v, w\}^T$ are displacement components in a rectangular Cartesian coordinate system.

3. MODELING RESULTS

To investigate the reduction in breaking stress caused by porosity, the effect of an artificial stress concentrator on stress development in three-point bend tests was modeled. According to the model the artificial stress concentrator localizes stress and causes a significant increase in stress (Figure 3). The modeled stress concentrator increased the local stress during the three-point bend test by a factor of four.

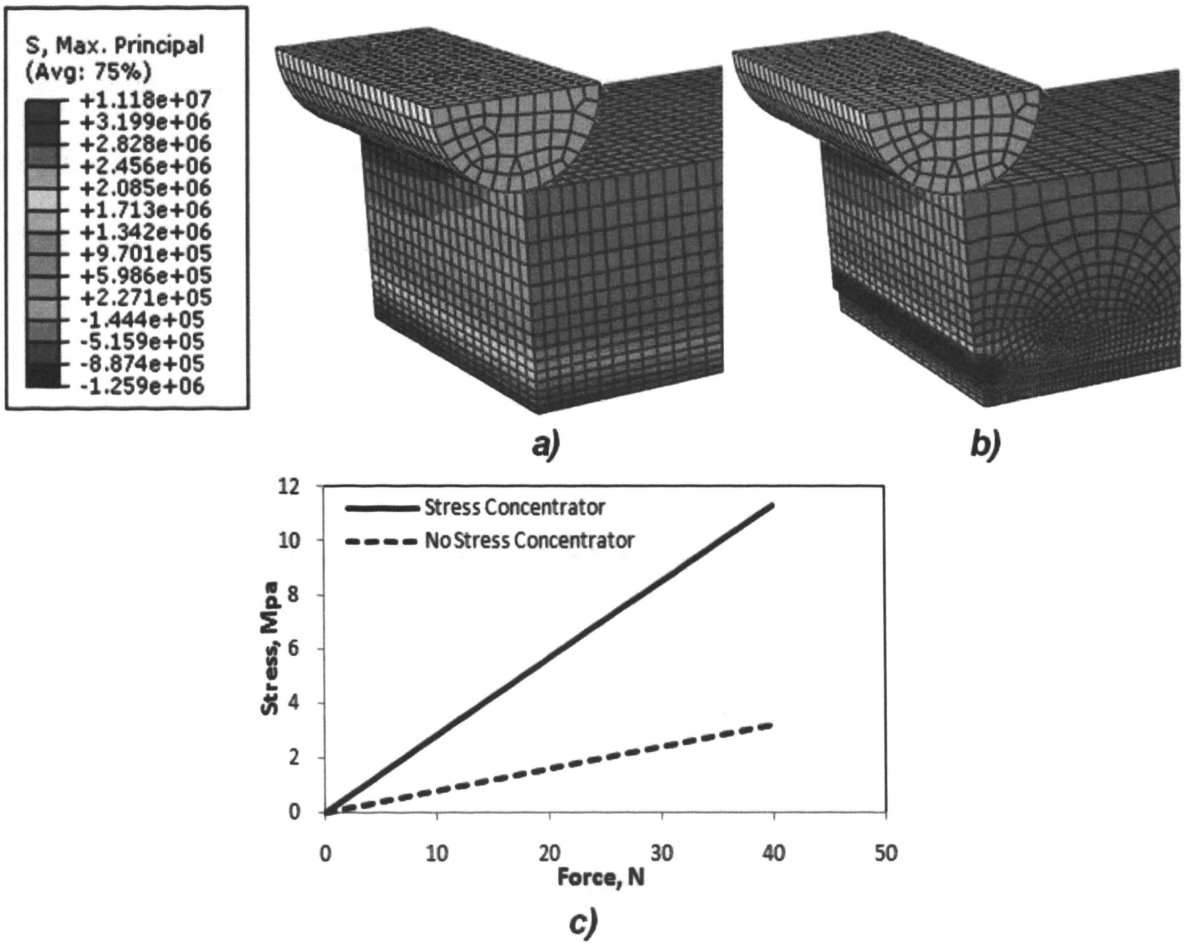

Figure 3. Illustration of calculated stress distribution in three-point bended specimen without (a) and with notch (b), and stress versus loading force for both cases (c).

To determine possible interactions between internal pores and corner radius during loading in the wedge specimen, a model of the wedge with a pore was developed (Figure 4a). Shell geometry and load were held constant with variation in corner radius (r). Decreasing r in the model without a pore exponentially increased stress concentration with an exponential power of -0.27. In the shell with a pore, decreasing r also increased stress concentration exponentially, but the exponential power decreased (Figure 4b). Larger pore radius (R) caused a more significant change because the area of stress concentration was larger. It was found that the relationship between r and stress shown by largest pore (0.75 mm R) was closest to the relationship of experimental samples as shown by no significant difference in the relationship of corner radius (r) and stress when modeling 0.5 R pores and 0.75 R pores. The cause of increased stress concentration with a pore present is the reduction in material at the corner of the shell. Because of this effect the large pore was assumed to have the same effect a multiple smaller pores. The exponential power used to correct for the interaction of pores and r was -0.16. When r is larger than R, stress concentration is controlled by the porosity. For smaller r values the pore had no significant effect because of the high stress concentration caused by the corner.

In addition to corner radius (r), the thickness (t), width (w), loading distance (d), and the angles θ and α were separately varied in the finite element model to determine their effect on the stress in the wedge for a given force. The results were used to formulate Eq. 5 that fits the modeling results for a fully dense ceramic:

$$\sigma = \frac{16.7Fd\cos(\theta - \alpha)r^{-0.27}}{Wt^2} \tag{5}$$

Presence of a single pore decreased the effect of radius on stress concentration (Figure 4b) and Eq. 5 was modified to account for this difference:

$$\sigma = \frac{20Fd\cos(\theta - \alpha)r^{-0.16}}{WT^2} \quad (6)$$

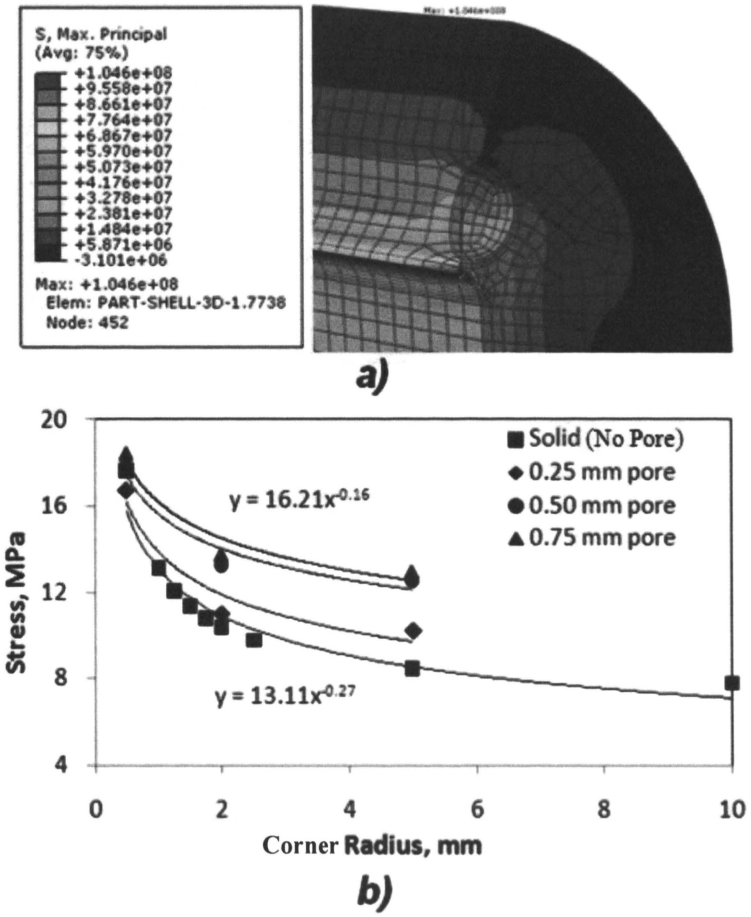

Figure 4. Illustration of calculated stress distribution in loaded wedge with 0.75 mm radius pore (a) and the effect of radius of wedge and pore on stress in shell at constant applied force and dimensions (b). Shows that as pore radius increases the difference between stress for different corner radii decreases.

The finite element modeling results for both the dense wedge model and the wedge model with a pore were compared to the values approximated from Eq. 5 and Eq.

6 as well as values obtained using previously published[7] Eq. 1 (Figure 5). The suggested equations take into consideration all geometric variables and are applicable to a greater range of possible geometries of wedge specimens with and without a pore, that have been modeled.

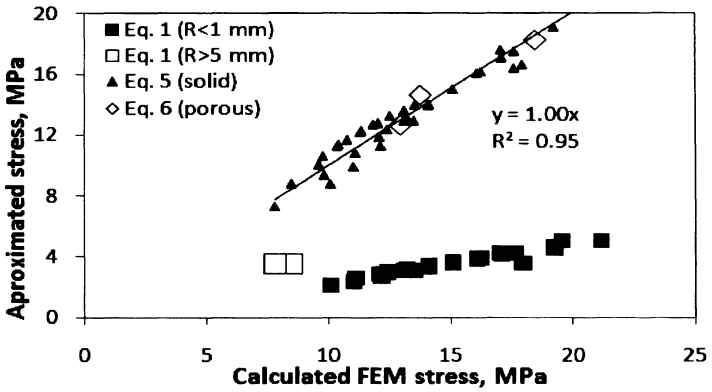

Figure 5. The relationship between the finite element modeling results and stress values calculated by Eq. 5 and Eq. 6 compared to Eq. 1.

4. EXPERIMENTAL RESULTS AND DISCUSSION

Microstructures of the various corner geometries were prepared to investigate the effect of microstructural features in the shell on its properties. In flat regions of the shell the various layers of shell can be seen and the fine stucco of the prime coat is fairly uniform and thick (Figure 6). Both corner images show similar structure to the flat region except for differences in the prime coat. The structure of a 5.0 mm radius corner is shown in Figure 6b and shows a uniform layer of prime coat stucco that is thinner than observed in the flat sample. The 0.5 mm radius corner shows almost no prime coat

stucco at the corner (Figure 6c). Elongated porosity with a radius of 0.2-0.7 mm can be observed in the images.

To determine the effect of internal porosity on the breaking stress of the shell both the experimental and modeling results of three-point bend testing with a stress concentrator were compared. The flexural failure stress was calculated from experimentally measured braking force (F) using:

$$\sigma = \frac{3Fl}{2WT^2} \tag{7}$$

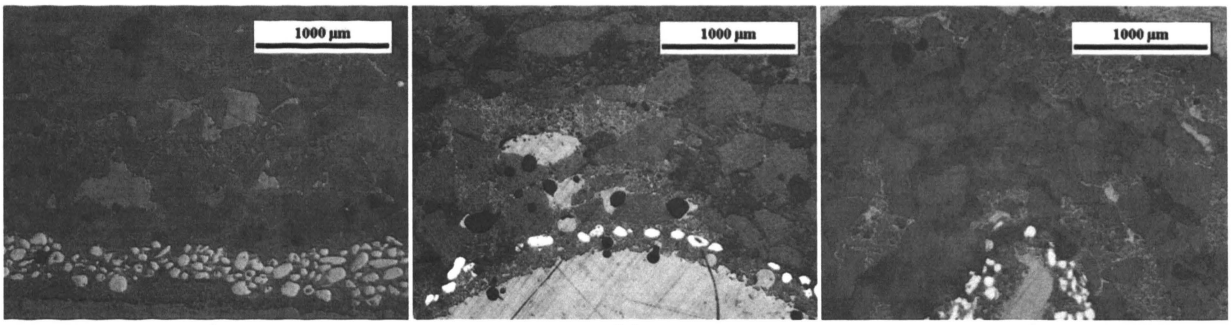

Figure 6. Microstructures of the investment casting shell in flat regions (a), and wedges with 5 mm (b) and 0.5 mm (c) corner radii that shows differences in the structure of the prime coat stucco.

Where: F is the applied force, l is the span length, W is sample width, and T is the sample thickness. The results from these tests were compared to the finite element modeling results (Table 1). The model shows that with constant force there is a large increase of stress in the shell with a notch but the experimental results show no significant difference in breaking stress. These results demonstrate that internal porosity is as significant a stress concentrator as the artificially added "notch".

Tests were performed on green shells and fired shells (1 hour @ 1000°C). The MCA model (Eq. 2) was applied to Eq. 6 to correct for the change in thickness caused by porosity. With this correction applied Eq. 6 becomes:

$$\sigma = k\frac{20Fd\cos(\theta - \alpha)r^{-0.16}}{WT^2} \quad (8)$$

Where: k is the correction value for porosity determined form the MCA model. Using the values of the stress from the three-point bend modeling cases with and without a stress concentrator and the volume percent porosity of the shells that were tested (0.3), the empirical parameter b in Eq. 2 was calculated to be 4.0. Using Eq. 2 the value of k was calculated to be 0.3. This lowers the failure stress from Eq. 7 to a range that fits with three-point bend test results (Figure 7a). Eq. 8 fits experimental data best when the maximum observed pore radius is smaller than the corner radius. When R is larger than r the model overestimates the fracture strength. To estimate breaking stress values for wedges with r values smaller than 2.0 mm it is recommended that the value of the r used in Eq. 8 should be 2.0 mm. By substituting a larger r value the resulting stress fits with expected values. When there is a high volume fraction of porosity near the inside corner of the shell, either caused by a higher number of pores or larger pores, the amount of stress concentration increases. Variation in the sample wedge angle causes a slight difference in strain rate in the fracture zone, this change in strain rate showed no significant effect on the breaking stress in the model or experimental results. Eq. 8 was applied to both fired and unfired samples and properties in flat and wedge regions were comparable for both cases (Figure 7b).

Table 1. Summary of modeling and experimental results for flat three-point bend test of flat specimen.

Case	Length, mm	Width, mm	Thickness, mm	Notch	Experimental flexural failure stress, MPa	FEM calculated flexural failure stress, MPa
1	76.2	29.0	7.1	Yes	3.7	11.3
2				No	3.7	3.2

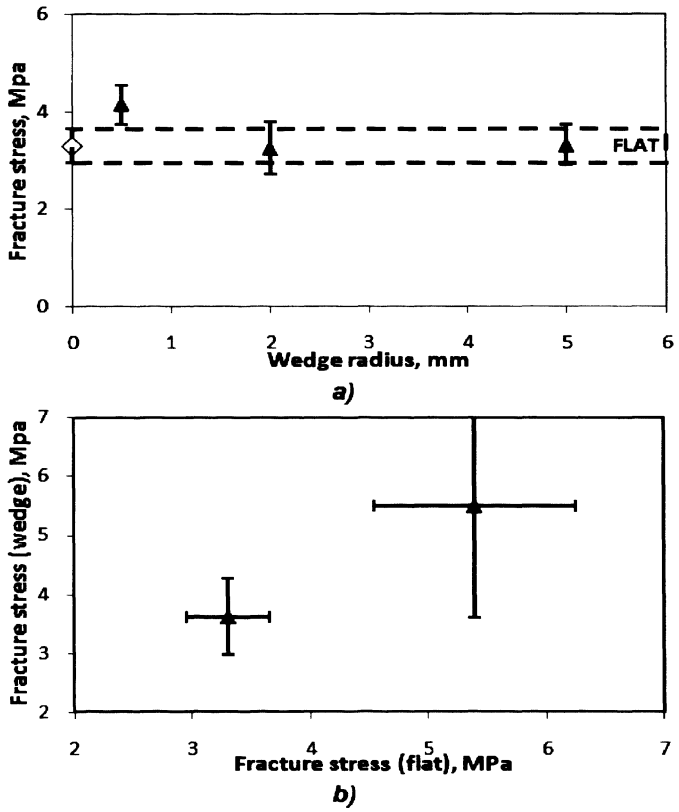

Figure 7. Comparison of fracture stress of "green" flat and wedge specimens with different radii (a) and comparison of fracture stresses for fired and unfired samples (b).

5. CONCLUSIONS

The strength of corner and edge regions was analyzed. Shell porosity was found to significantly reduce the effect of corner radius on the amount of stress concentration.

Experimental methods were combined with finite element modeling to develop the following equation to predict stress in corner regions of the shell:

$$\sigma = k\frac{20Fd\cos(\theta - \alpha)r^{-0.16}}{WT^2} \quad (8)$$

Eq. 8 predicts stress accurately for corner radii 2.0 mm or larger. The results from the model were experimentally verified after using the MCA model (Eq. 2) to adjust stress values for the effect of porosity. The failure stress of flat and corner regions of the shell were found to be similar for both fired and un-fired shells.

ACKNOWLEDGEMENTS

The authors would like to thank US Army ARDEC - Benet Labs for funding this research under contract number W15QKN-07-2-0004. The authors wish to recognize the assistance of Tom Towey, Katherine Ramsey and Jamie Fitzgerald for sample preparation. The results and opinions contained in this paper are those of the authors and not necessarily those of U.S. Army Benet Labs.

REFERENCES

1. Foster, G, "Flashfire Dewax for Today's Investment Casting Foundry", Investment Casting Institute 42nd Annual Meeting, pp. 2:1-2:11, Atlanta, Georgia; USA; 25-28 September 1994.

2. Yao, W L; Leu, Ming C, "Analysis of Shell Cracking in Investment Casting with Laser Stereolithography Patterns", Rapid Prototyping Journal, Vol. 5, no. 1, March 1999.

3. Capadona, J A, "Slurry Process Control in Production can "Crack Down" on Shell Cracking", Incast Vol. 4, no. 4 pp. 10-12, April 1991.

4. Guerra, M, Schiefelbein, G W, "Review of Shell Components, Shell Characteristics and Properties: Refractory Selection for Primary Shell Coat", Investment Casting Institute 42nd Annual Meeting, Atlanta, Georgia; USA; 25-28 September 1994.

5. Darryl Kline, Controlling Strength and Permeability of Silica Investment Casting Molds, Missouri University of Science and Technology, Thesis 2010, pp 46-47.

6. Kline, D, Lekakh, S, Mahimkar, C, Richards, V, "Crack Formation in Ceramic Shell During Foam Pattern Firing", Technical and Operating Conference, Chicago, Illinois; USA; December 2009.

7. Hyde, R, Leyland, S, Withey, P, Jones, S, "Evaluation of the Mechanical Properties of Investment casting Shells", 22nd Investment Casting Conference, 1995.

8. Peterson, R E, "Peterson's Stress Concentration Factors", John Wiley and Sons Inc., pp. 18-20, 1961.

9. Kruse, B L, Richards, V L, "Thermal and Moisture Characterization During Autoclave Dewaxing in Investment Casting", Proceedings of the 59th SFSA T&O Conference, No. 5.5, 2005.

10. Chirag Mahimkar, Thermo-physical Properties Measurement and Steel- Ceramic Shell Interactions in Investment Casting, Missouri University of Science and Technology, Thesis 2011, pp 76.

11. Nyongesa, F W, Aduda, B O, "Fracture Strength of Porous Ceramics: Stress Concentration vs Minimum Solid Area Models", African Journal of Science and Technology, Science and Engineering Series, Vol. 5, no. 2, pp 19-27, December 2004.

12. ASTM C1161, "Standard Test Method for Flexural Strength of Advanced Ceramics at Ambient Temperature", ASTM International, 2002.

13. ASTM C20, "Standard Test Methods for Apparent Porosity, Water Absorption, Apparent Specific Gravity, and Bulk Density of Burned Refractory Brick and Shapes by Boiling Water", ASTM International, 2000.

14. ABAQUS Version 6.9. Manual, Dassault Systèmes, 2009.

2. CONCLUSIONS

This thesis is a collection of papers that discuss shell cracking in investment casting during pattern removal. The first two papers discuss the factors affecting shell cracking and methods to prevent it. The third paper discusses the strength of investment casting shells in corner regions.

In the first two papers the mechanism of crack formation in investment casting ceramic shells during rigid polymeric foam pattern removal was analyzed. A model was developed for predicting crack formation in investment casting shells due to pattern expansion. The model takes into consideration the thermal and mechanical properties of the pattern and shell materials to determine the heat transfer and thermal expansion stresses developed in the shell during firing. The model shows that increasing foam density, elastic modulus, and foam softening temperature increase the chance of shell cracking. Increasing the shell strength and thickness decrease the chance of shell cracking. The effect of polyurethane foam pattern aging after shell fabrication on crack formation in investment casting ceramic shells during pattern removal was also analyzed. Aging reduces the stress in the shell by producing shrinkage which lowers the compatibility strain on heating and its consequent elastic stress development. The effect of pattern aging on shell cracking during pattern removal was applied to the model. The model shows that foam aging reduced the amount of pattern expansion during pattern removal.

The model accurately predicts the presence of cracking during pattern removal. The results of the model and the experiments demonstrate that patterns should be made with lower density polyurethane foam in order to prevent shell cracking during pattern

removal. It is also recommended that the pattern should be removed using flash firing at 600°C or higher. To effectively prevent shell cracking, pattern aging can be done above the first glass transition temperature (60°C) for at least 24 hours.

The strength of corner and edge regions was analyzed. Shell porosity was found to significantly reduce the effect of corner radius on the amount of stress concentration. Experimental methods were combined with finite element modeling to develop the following equation to predict stress in corner regions of the shell:

$$\sigma = k\frac{20Fd\cos(\theta - \alpha)r^{-0.16}}{WT^2} \tag{8}$$

Eq. 8 predicts stress accurately for corner radii 2.0 mm or larger. The results from the model were experimentally verified after using the MCA model (Eq. 2) to adjust stress values for the effect of porosity. The failure stress of flat and corner regions of the shell were found to be similar for both fired and un-fired shells.

Additional work should be done on larger more complicated patterns to provide a more realistic approximation of industrial practice. The application of the model to industrial shells should be investigated to verify that a wide range of shell properties can applied to the shell cracking model. More aging tests should be done to more accurately determine the activation energy of aging as well as the mechanism of aging. Further investigation of the properties in shell corners should be done to improve the wedge strength model and its application to corner radii smaller than 2.0 mm. A new standard procedure for the wedge strength model should be developed.

VITA

The author, Wesley Alexander Everhart, was born on April 26, 1987 in Kansas City, Kansas to Michael and Janette Everhart. He graduated from Shawnee Mission West High School in May of 2005. After graduation, he went on to receive his baccalaureate in Metallurgical Engineering from the Missouri University of Science and Technology in May of 2009.

This publication is the culmination of his Master of Science in Metallurgical Engineering, which he earned in December 2011 at the Missouri University of Science and Technology under Dr. Von L. Richards.